Iranian Journal of Materials Science and Engineering, Vol. 19, Number 2, June 2022
RESEARCH PAPER

Specifications of Biodegradable Restricted PCL and PLLA Chains in Biocompatible PEG-*b*-PCL and PEG-*b*-PLLA Single Crystals

Saleheh Abbaspoor[1], Farhang Abbasi[1], Samira Agbolaghi[2]

* *abbaspoor.polymer@gmail.com*

[1] Institute of Polymeric Materials and Faculty of Polymer Engineering, Sahand University of Technology, Tabriz, Iran
[2] Chemical Engineering Department, Faculty of Engineering, Azarbaijan Shahid Madani University, Tabriz, Iran

Received: January 2021 **Revised: July 2021** **Accepted: November 2021**

DOI: 10.22068/ijmse.2132

Abstract: *Single crystals of double crystalline block copolymers of poly (ethylene glycol) (PEG)-b-poly(ε-caprolactone) (PCL) and PEG-b-poly(L-lactide) (PLLA) were grown from dilute solution in homo- and mixed-brush systems. Crystallization behavior of biodegradable one end-restricted crystallizable PCL and PLLA chains in homo- and mixed-brush nanostructures were investigated. The chemical and physical circumstances of crystallizable brushes were altered. The physical environment was adjusted by amorphism/crystallinity and rigidity/ flexibility of neighboring brushes. The chemical environment was manipulated by interaction and miscibility of various brushes. Distinct single crystals were grown with mixed-brushes of amorphous-crystalline (polystyrene (PS), poly (methyl methacrylate) (PMMA), PCL, PLLA, double crystalline (PCL/PLLA), and rod-crystalline polyaniline (PANI)/PCL or PLLA. Surrounding was only effective on hindrance or nucleation commencement of crystallization for crystallizable brushes and had no effect on crystallization features. Novel three-layer fully single-crystalline nanostructures, whose characteristics were fixed via changing the crystallization temperature, were also developed. For long crystallizable tethers, crystallization increased both brush and substrate thicknesses.*

Keywords: *Restricted crystallizable chain, double crystalline block copolymer, single crystal.*

1. INTRODUCTION

Compared to the amorphous-crystalline block copolymers, some limited studies were devoted to the single crystallization of double crystalline block copolymers [1–3]; because the latter ones were more complicated. The double crystalline block copolymers are categorized into two sorts. (1) The block copolymers possessing similar melting points such as poly(4-methyl-1-pentene)-*block*-poly(l-lactide) (sPMP−PLLA); (2) the block copolymers with conspicuously different melting points like polyethylene (PE)-*b*-poly(3-butylthiophene) (P3BT) and PEG-*b*-poly(3-hexylthiophene) (P3HT) [1–5]. In research, the block with the larger molecular weight, first crystallized, and the other block became either amorphous or crystallized in a proper condition in the dilute solution grown PEG-*b*-PCL single crystals [6–9]. Van Horn et al. [8] altered the crystallization priority by selecting the appropriate solvents and homopolymer seeds, which were determined by the weight fraction of various blocks. To the best of our knowledge, the studies on the single crystals of PEG-*b*-PLLA block copolymers have only been developed in the melt state [1–3]. In addition to the mentioned parameters, our solution crystallization studies on these double crystalline block copolymers indicated that the chemical and physical circumstances and the crystallization procedure could determine the crystallization behavior of crystallizable tethered chains and crystallization sequence of crystalline-crystalline block copolymers [4–5, 10].

Block copolymers with biodegradability, biocompatibility, and amphiphilicity such as PEG-*b*-PCL and PEG-*b*-PLLA have attracted significant attention because of their enormous applications in the biotechnology, biomedical, and biodegradation areas subsuming the drug delivery systems, implantation, wound healing, tissue engineering, and responsive hydrogels [11–21]. The crystallization behavior of these double crystalline block copolymers determines the final biodegradability and biocompatibility properties in the respective applications [19]. Therefore, the recognition of single crystallization of these biocompatible/ biodegradable double crystalline block copolymers is very important.

In the current work, through the growth of PEG-*b*-PCL and PEG-*b*-PLLA single crystals from

[Downloaded from isee.iust.ac.ir on 2025-07-27]

[DOI: 10.22068/ijmse.2132]

dilute solution, the crystallization behavior and properties of crystallizable PCL and PLLA brushes in homo- and mixed-brushes were investigated. In more detail, the crystallization circumstance of PEG substrate and PCL/ PLLA brushes, as well as their mutual effects on the crystallization, were studied. The influences of surrounding properties on the nucleation and crystallization of crystallizable brushes and substrate were also investigated. The chemical the environmental influence was studied in the realm of interactions of crystallizable brushes with the surrounding brushes. The physical environmental effect was also covered by the amorphism or crystallinity and rigidity or flexibility of neighboring brushes. In more details, by using different environments, the crystallization behavior of crystallizable brushes was manipulated, and thereby the corresponding crystallization properties were studied in various conditions. To this purpose, the homo-brush single crystals sandwiched between the crystallizable PCL and PLLA brushes using different diblock copolymers including the blocks of PEG, PCL, PLLA, PS, PMMA and PANI were designed and employed to study the effective parameters. It is the first time that the single crystal specifications of crystallizable polymers in state of one-end restricted (tethered) chains were investigated. Effects of various parameters on the formation and properties of tethered chain single crystals were comprehensively studied. Parameters were composed of brush type, molecular weight, interactions with respect to surrounding environment and substrate, etc.

2. EXPERIMENTALPROCEDURE

The atom transfer radical polymerization (ATRP) was utilized to synthesize the PEG_{5000}-*b*-PS [22–24] and PEG_{5000}-*b*-PMMA [23, 24] copolymers with the dispersity ranges of 1.11−1.18 and 1.20− 1.22, respectively. The PEG_{5000}-*b*-PANI copolymers were synthesized by an interfacial polymerization with potassium hydrogen biiodate (PHD) as a dopant [25]. The PEG_{5000}-*b*-PCL [25, 26] and PEG_{5000}-*b*-PLLA [28, 29] diblock copolymers were also synthesized by the ring-opening polymerization (ROP), possessing the dispersities ranged in 1.22− 1.26 and 1.21− 1.24, respectively. The solution crystallization was performed with a concentration of 0.018 wt% and the ratio of 50:50 wt:wt for the mixed block copolymers in amyl acetate (Merck, >98%) based on the self-seeding procedure [23]. The concentration of homopolymer systems was also 0.009 wt%. The sample was put into a cell tube containing the solvent, and, subsequently, the cell tube was purged, sealed, and kept at the dissolution temperature (T_d= 70°C) for 35 min. The cell tube then passed the primary crystallization (at 0°C for 6 h) and self-seeding (T_s= 41°C for 20 min) steps. It was then switched to the desired crystallization temperature (T_c) and maintained for 2– 3 days. The atomic force microscope (AFM Nanoscope), scanning transmission electron microscopy (STEM), electron diffraction mode of the transmission electron microscope (Philips CM30 TEM), and small-angle X-ray scattering (CMOS flat-panel SAXS detector (C9728DK)) measurements were applied to analyzed the designed single crystals. Thermal data points were gathered by the differential scanning calorimetry (DSC) (NETZSCH, F3 Maia200) (Fig. S5).

3. RESULTS AND DISCUSSION

For the crystallization of crystallizable polymers, nucleation, suitable mobility, and the interaction of polymer chains are needed. Herein, the surrounding environment affected the polymer chain interactions and thus the possibility of nucleation for the crystallization of polymer chains. After nucleation, the mobility of attaching polymer chains to the nucleus determines the crystallization procedure and rate. The crystallizable polymer brushes had one restricted end chain, which was tethered on the substrate. For the single crystallization of double crystalline block copolymers, each block thatcould crystallize first fabricated the substrate, and the other one formed the brushes. In upcoming sections, the surrounding environmental effects from the viewpoints of chemical and physical issues will be discussed on the nucleation and crystallization circumstance of crystallizable substrate and brushes.

4. CRYSTALLIZABLE BRUSHES IN HOMO-BRUSH SYSTEMS

The single crystals of PEG_{5000}-*b*-PCL_{4700}, PEG_{5000}-*b*-PCL_{9100}, PEG_{5000}-*b*-$PLLA_{7800,}$ and

[Downloaded from isee.iust.ac.ir on 2025-07-27]

[DOI: 10.22068/ijmse.2132]

PEG_{5000}-*b*-$PLLA_{13300}$ block copolymers were grown from amyl acetate dilute solution. On the basis of selected area electron diffraction (SAED) patterns as well as the morphologies verified by the AFM, STEM, and TEM images, in all grown single crystals, the PEG blocks composed the substrate, and the second blocks developed various crystalline and amorphous brushes. To investigate the crystallization behavior of crystallizable brushes grafted on the substrate surface, the SAED patterns were recorded. In addition to the [120] growth prism belonging to the PEG crystalline structure in SAED patterns, the square lateral habit of developed single crystals demonstrated that the PEG blocks were entered into the crystalline structure of the substrate. The appearance of [110] and [200] prisms also demonstrated the crystallinity of PCL and PLLA grafted brushes (Figs. 1– 6, 8). In more details, the four spots were $(120)_{PEG}$, owing to the monoclinic lattice structure of the PEG crystal (a= 0.805 nm, b= 1.304 nm, c= 1.948 nm and α= γ = 90°, β= 125.4°) [30]. In addition, the prisms of $(200)_{PCL}$ and $(110)_{PCL}$ were detected in the PCL crystals (a= 0.747 nm, b= 0.498 nm, c= 1.705 nm and α= β = γ = 90°) because of their orthorhombic lattice structure [31]. Owing to the orthorhombic α-form of PLLA crystals (a= 1.07 nm, b= 0.595 nm, c= 2.78 nm and α= β = γ = 90°), the growth planes of $(200)_{PLLA}$ and $(110)_{PLLA}$ appeared [32]. These results indicated a flat-on orientation for the chains constructed by both substrate and brush single crystals.

In the PEG_{5000}-*b*-PCL_{9100} single crystals, the PEG and PCL blocks had a similar melting point. AFM height images and the corresponding SAED patterns of PEG_{5000}-*b*-PCL_{9100} single crystals grown at 28°C and 39°C are represented in Figs. 1(a) and (b), respectively, in which the PCL brushes were crystalline. In spite of higher molecular weight of PCL, due to a poorer quality of amyl acetate for the PEG compared to PCL, the PEG chains had a higher priority for the crystallization and, consequently, the fabrication of single-crystal substrate. It was well consistent with the previous studies [5, 8–9]. First, the crystallization of PEG blocks could be occurred in the PEG-*b*-PLLA single crystals because of the crystallization procedure. In fact, by operating below 70°C (higher than the dissolution temperature of PEG and lower than that of PLLA), only the PEG blocks could be crystallized to construct the final single crystalline substrate. This was in opposition with that dictated by the quality of solvent with respect to PEG and PLLA. In the range of processing temperatures, the amyl acetate was a very poor [33, 34] and poor solvent for the PLLA and PEG blocks, respectively. Therefore, the PLLA chains were tethered as the polymer brushes on the PEG substrate. Furthermore, the crystallization of crystallizable PCL and PLLA brushes, which had one restricted end chain, was focused. In the PEG_{5000}-*b*-PCL_{4700} single crystals, the PCL_{4700} brushes were crystallized at 39°C. The reason for the crystallization of crystallizable brushes at the higher temperature was the sufficient interactions between the tethered chains and their stretching, leading to the occurrence of nucleation. The single crystalline thickness of PCL brushes and PEG substrate were 4.76 and 4.80 nm, respectively. The height of PCL_{4700} brushes and the substrate thickness beneath them at T_c= 28°C, in which the grafts were amorphous, were 2.70 and 5.05 nm, respectively. Hence, it could be observed that through the incorporation of brushes into the single crystalline structure, their thickness increased; however, the substrate thickness decreased. This could be attributed to the difficulty of crystallization of short PCL_{4700} brushes and also their low osmotic pressure on the substrate in the amorphous state. In more detail, the grafted polymer brushes in the amorphous state exert an osmotic pressure on the substrate based on their dimension and compactness. It is important how the brushes crystallized because the crystallization of substrate and brushes simultaneously occurred. Hence, it affected the crystallization specifications of the brush and substrate single crystals. The thickness variation trends of PEG substrate and PCL_{4700} crystallizable brushes with respect to crystallization temperature are depicted in Fig. 1(c).

Thanks to the difficulty of crystallization for the short PCL_{4700} brushes, their crystallization was slow. Hence, the crystals with the larger folding numbers were reached for the PCL blocks, and consequently, the foldings of PEG substrate increased in the crystalline state of PCL brushes compared to their amorphous state. The approximate folding of PCL_{4700} brushes in the single crystals having the thickness of 4.76 nm and the extended length of 35.15 nm [10] was around 7. In fact, the substrate thickness

[Downloaded from isee.iust.ac.ir on 2025-07-27]

[DOI: 10.22068/ijmse.2132]

decreased in the crystalline state of PCL chains compared to their amorphous state (5.05 versus 4.80 nm). In the PEG_{5000}-*b*-PCL_{9100} single crystals, the PCL_{9100} brushes were crystallized at T_c= 28°C. It could be originated from the facile crystallization of higher molecular weights due to an increase in the interactions between the polymer brushes and their stretching. After incorporation of PCL_{9100} tethered chains into the crystalline structure, the thicknesses of PEG substrate and PLLA brushes were higher compared to those detected for the corresponding amorphous brushes (4.8 versus 2.5 nm and 9.18 versus 4.11 nm, respectively). This could be correlated with the higher tendency of brushes to crystallization and their larger osmotic pressure in the amorphous state. As an interesting point, the characteristics, including the thickness of the substrate and brush's single crystals, were similar at 28 and T_c= 39°C. Actually, when the single crystals of grafted brushes were developed at a given crystallization temperature, their properties maintained constant even at the higher crystallization temperatures.

The single crystalline thicknesses of PCL_{9100} brushes and their substrate at 28°C were 9.13 and 4.80 nm and at 39°C were 9.10 and 4.77 nm, respectively. When the grafted brushes were crystallized, the simultaneous crystallization of substrate and brushes components affected each other, and the ultimate features of the substrate and brush single crystals were determined. Therefore, the results of various effects on the free energy of the system determined the equilibrium thickness of the substrate and brush single crystals. Via an elevation in the crystallization temperature of the amorphous state brushes, the substrate thickness increased up to where allowed by the brush regime and their osmotic pressure.

By providing the crystallization condition for the crystallizable brushes at a given temperature, via temperature elevation, the properties of grown single crystals did not change anymore. In fact, the novel three-layer sandwiched single crystals were developed whose features were fixed. It means that the equilibrium condition was determinant on the characteristics of the substrate and brush single crystals, and at the higher temperatures, thanks to the correlation between the crystallization of various components, a similar equilibrium condition maintained the thicknesses. As another point, with an enhancement in the molecular weight of PCL brushes from 4700 to 9100 g/mol, only the thickness of brushes single crystals increased, and their folding number and also the PEG substrate thickness were constant. Furthermore, the folding number of crystalline brushes in their single-crystalline structures determined the exerted osmotic pressure on the PEG substrate and thus its thickness. Fig. 1 represents AFM height images and the corresponding SAED patterns of PEG_{5000}-*b*-PCL_{9100} single crystals prepared at T_c= 28°C and T_c= 39°C. The variation trends of PEG substrate and PCL_{9100} crystallizable brush thicknesses versus the crystallization temperature are also reported in the bar graphs of Fig. 1(c).

In more detail, the PCL_{4700} brushes with an extended length of 35.15 nm and the crystal thickness of 4.76 nm possessed 7 foldings. On the other hand, the PCL_{9100} brushes having an extended length of 68.05 nm and the crystal thickness of 9.13 nm had a similar folding number (~7). This phenomenon could be ascribed to the fact that the molecular weight enhancement of polymer brushes and, consequently, the facilitation of their crystallization not only provides the crystallization condition for them at lower temperatures but also accelerates the crystallization compared to the shorter brushes. In these growth systems, the crystallization condition was provided when the nucleation barriers were overcome. Parallel with an enhancement in the crystallization rate, only the thickness of crystallizable brush crystals increased, whereas the folding and thus the PEG substrate thickness remained constant.

By altering the crystallizable brushes from PCL to PLLA, in the PEG_{5000}-*b*-$PLLA_{7800}$ single crystals, the PLLA brushes were amorphous at a whole range of crystallization temperatures. It was because of the high miscibility between the PEG substrate and PLLA brushes. It resulted in the prohibition of sufficient interactions between the short $PLLA_{7800}$ chains thereby they could not be crystallized. However, by increasing the molecular weight of PLLA brushes from 7800 to 13300 g/mol, they were crystallized at T_c= 28°C. Actually, the appropriate interaction of long $PLLA_{13300}$ chains and their stretching prevail over the substrate and brush attractions. Hence, the crystallizable brushes could be crystallized.

[Downloaded from isee.iust.ac.ir on 2025-07-27]

[DOI: 10.22068/ijmse.2132]

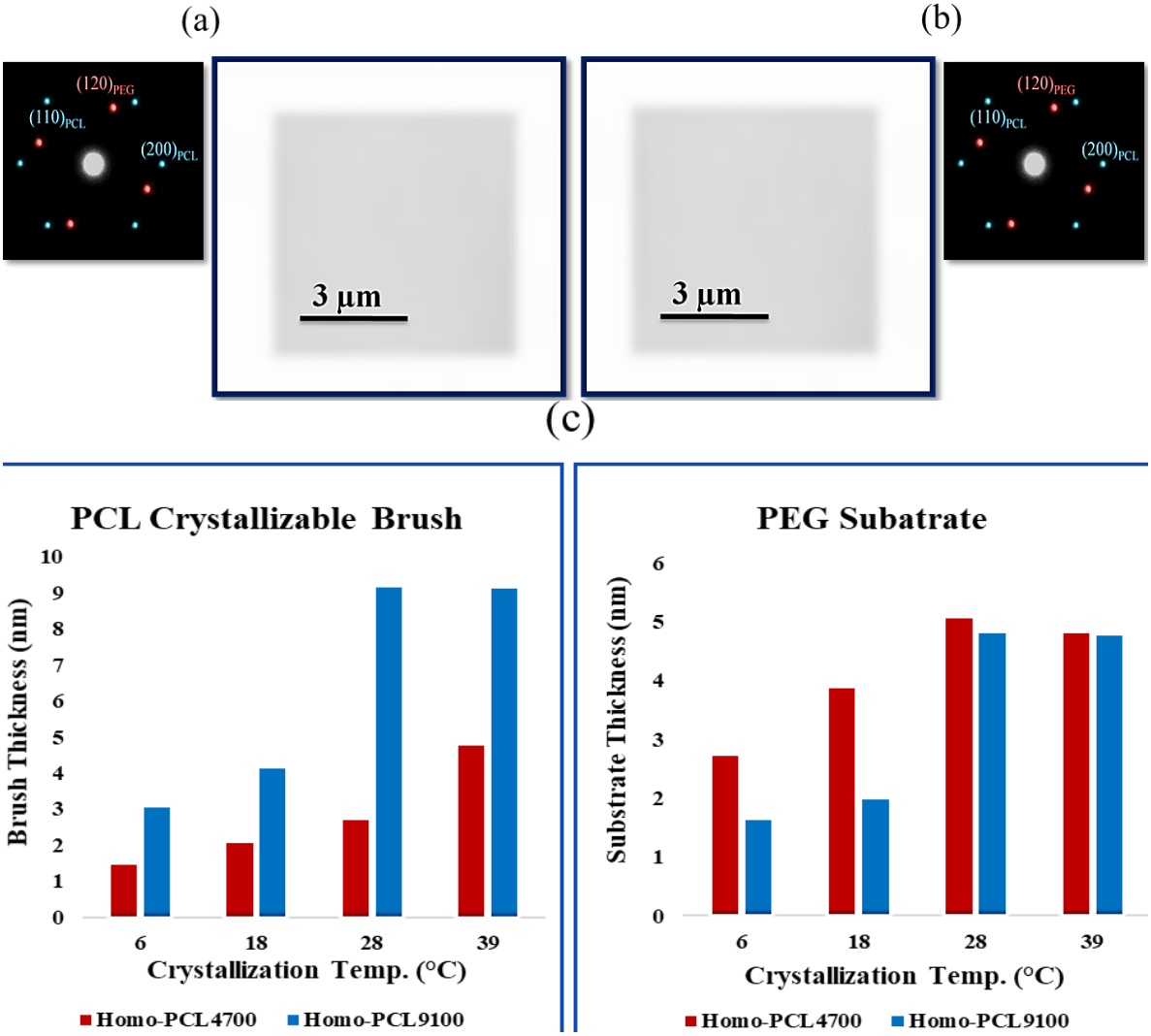

Fig. 1. AFM height images and the corresponding SAED patterns of PEG5000-b-PCL9100 single crystals grown at Tc = 28°C [5] (a) and T_c= 39°C (b), in which the PCL brushes are crystalline; the thickness trends of PCL brushes and PEG substrate via altering the crystallization temperature in PEG5000-b-PCL4700 and PEG5000-b-PCL9100 single crystals (c).

Similar to the long length of PCL-based systems, the developed single crystals from the PLLA brushes retained their characteristics even at higher crystallization temperatures. The thickness of $PLLA_{13300}$ crystals and their PEG substrate at 28°C were 17.75, 6.4 nm, and at 39°C were 17.72 and 6.44 nm, respectively. In these brushes, in contrast to the PCL_{4700} brushes and similar to PCL_{9100} ones, after the incorporation of tethered chains into the crystalline structure, the PEG substrate and PLLA brush thicknesses were higher compared to those detected for the corresponding amorphous brushes. As mentioned previously, this could be correlated with the higher tendency of $PLLA_{13300}$ brushes to crystallization and their larger osmotic pressure in the amorphous state. The facile crystallization of $PLLA_{13300}$ brushes could reflect a faster crystallization, and thereby the lower foldings in both brush and substrate crystals. As above-mentioned, due to the simultaneous crystallization of substrate and brushes, the crystallization of brushes affected the characteristics of PEG substrate underneath them. Figs. 2(a) and (b) display AFM height images and the corresponding SAED patterns of PEG_{5000}-*b*-$PLLA_{13300}$ single crystals prepared at T_c= 28 and 39°C. The thickness trends of PEG substrate and $PLLA_{13300}$ crystallizable brushes with respect to the crystallization temperature are also shown in Fig. 2(c).

In upcoming sections, by adding different brushes, the neighboring environment of

[Downloaded from isee.iust.ac.ir on 2025-07-27]

[DOI: 10.22068/ijmse.2132]

crystallizable brushes will be altered. Hence, the crystallization behavior of crystallizable tethers could be exactly adjusted. The circumstance effects on the brush crystallization properties and the universality of the obtained results in the homo-brush systems were also investigated.

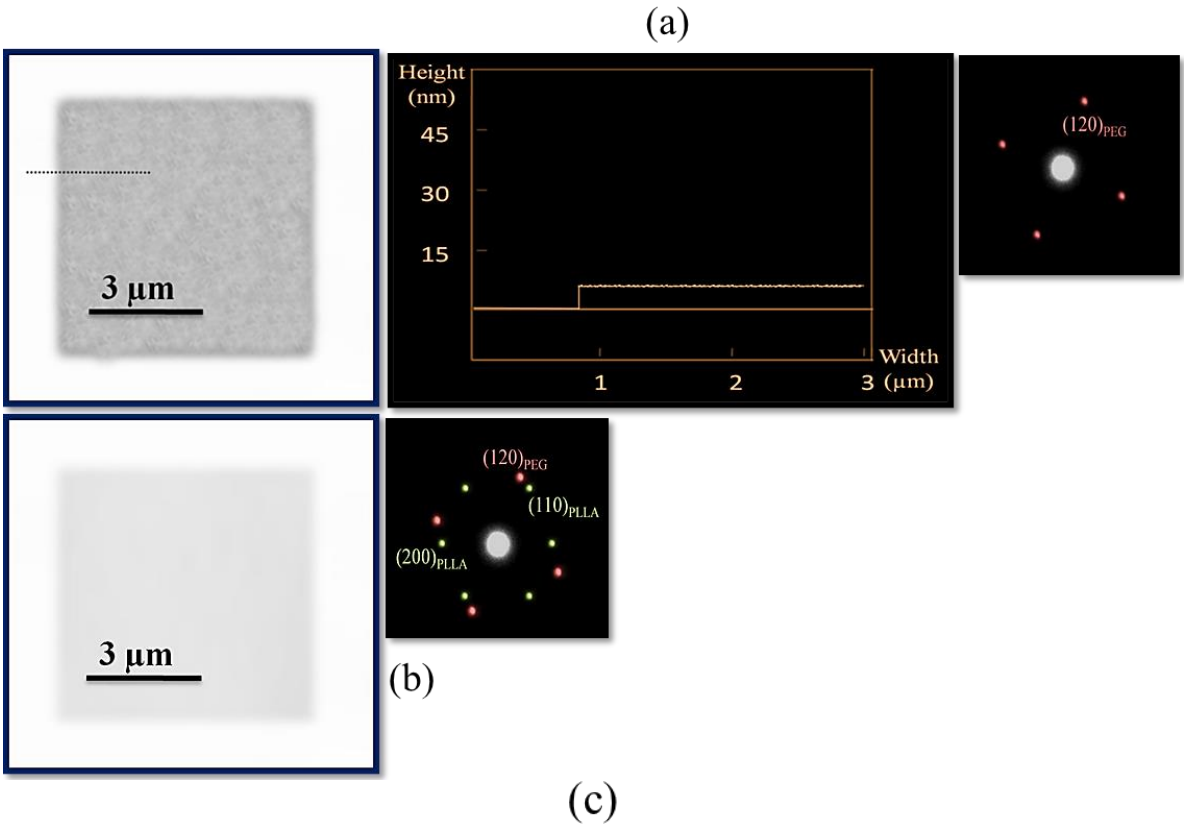

Fig. 2. AFM height image, height profile, and the corresponding SAED pattern of PEG5000-b-PLLA13300 single crystals grown at T_c= 6°C (a), in which the PLLA brushes are amorphous; AFM height image and the corresponding SAED pattern of PEG5000-b-PLLA13300 single crystals grown at T_c= 39°C (b), in which the PLLA brushes are crystalline; the thickness trends of PLLA brushes and PEG substrate versus the crystallization temperature in PEG5000-b-PLLA7800 and PEG5000-b-PLLA13300 single crystals (c).

[Downloaded from isee.iust.ac.ir on 2025-07-27]

[DOI: 10.22068/ijmse.2132]

5. CRYSTALLIZABLE BRUSHES IN THE VICINITY OF PS BRUSHES

In the mixed-brushes resulting from the PEG_{5000}-*b*-PS_{18500}/PEG_{5000}-*b*-PCL_{4700} single crystals, the PCL_{4700} brushes with the repulsive interaction with the PS neighboring brushes [35] were crystallized at a lower temperature (i.e., 28°C) compared to their corresponding homo-brushes. In more detail, the repulsive interactions between the PS and PCL brush led to the approaching of PCL brushes together and, consequently, resulted in the higher interactions between the PCL tethered chains, which finally caused their easier entrance into the crystalline state. With a decrease in the crystallization temperature for brushes, the single crystal properties were altered. At T_c= 28°C, thanks to a decrease in the commencement of nucleation temperature and brush crystallization, the thicknesses of substrate and brush crystals were lower, i.e., 3.09 and 3.14 nm, respectively. Similar to the homo-brush single crystals obtained from the long crystallizable tethers, these characteristics were also maintained even at the higher crystallization temperatures. So, it could be concluded that the molecular weight or chain length of crystallizable brushes did not have any impact on this observation.

The thicknesses of substrate and brush crystals at T_c= 39°C were 3.11 and 3.17 nm, respectively. In these mixed-brush systems, similar to the homo-brush systems, through the incorporation of crystallizable PCL_{4700} brushes into the single crystalline structure, their thickness increased; however, the substrate thickness decreased. As above-mentioned, this could be attributed to the difficulty of crystallization for the short PCL_{4700} brushes and also their low osmotic pressure on the substrate in the amorphous state. Hence, the presence of PS brushes caused the higher interactions between the PCL brushes and thus their easier entrance into the crystalline state at a lower temperature. The presence of PS brushes also facilitated the nucleation of PCL_{4700} brushes and, consequently, their commencement crystallization at lower temperatures. On the other hand, the osmotic pressure of brushes was less at lower temperatures. By large, the ratio between the crystallization rate and osmotic pressure of crystallizable brushes did not change in the crystalline and amorphous states. The thickness trends of PEG substrate and PCL_{4700} crystallizable brushes versus the growth crystallization temperature in the homo- and mixed-brush systems are also illustrated in Fig. 3(c).

By increasing the PCL molecular weight from 4700 to 9100 g/mol, in the PEG_{5000}-*b*-PS_{18500}/ PEG_{5000}-*b*-PCL_{9100} mixed-brush single crystals, the crystallization of PCL_{9100} brushes was detected at 18°C, which was lower than that was observed for the corresponding homo-brush systems. The thicknesses of the substrate and brush single crystals at T_c= 18°C were 3.08 and 6.07 nm, respectively, which were also retained even at the higher crystallization temperatures similar to the previous systems.

Due to repulsive interactions between the PS and PCL brushes, the presence of PS brushes just induced the crystallization and facilitated the entrance of crystallizable brushes into the single crystals.

The developed single crystals from the crystallizable brushes also maintained the properties at the higher crystallization temperatures. In addition, the molecular weight of crystalline brushes only affected the thickness of single crystals composed of crystallizable brushes, whereas their folding and thus the PEG substrate thickness remained constant. Via altering the molecular weight of PCL brushes from 4700 to 9100 g/mol, their single-crystal thicknesses increased from 3.14 to 6.07 nm. Regarding, the corresponding extended lengths (35.15 and 68.05 nm), the folding number in both mentioned crystals was ~11. Hence, in these mixed-brush systems, the previous results in the homo-brush systems were exactly verified. It represented that the induction influence of PS brushes just affected the crystallization commencement of restricted crystallizable brushes at the lower temperatures, and they did not have any impact on the crystallization characteristics of crystallizable brushes. Figs. 3(a−c) display the AFM height images and the corresponding SAED patterns of PEG_{5000}-*b*-PS_{18500}/PEG_{5000}-*b*-PCL_{9100} single crystals prepared at 6 and 39°C as well as the thickness trends of PEG substrate and PCL crystallizable brushes with respect to the crystallization temperature in homo- and mixed-brush single crystals.

[Downloaded from isee.iust.ac.ir on 2025-07-27]

[DOI: 10.22068/ijmse.2132]

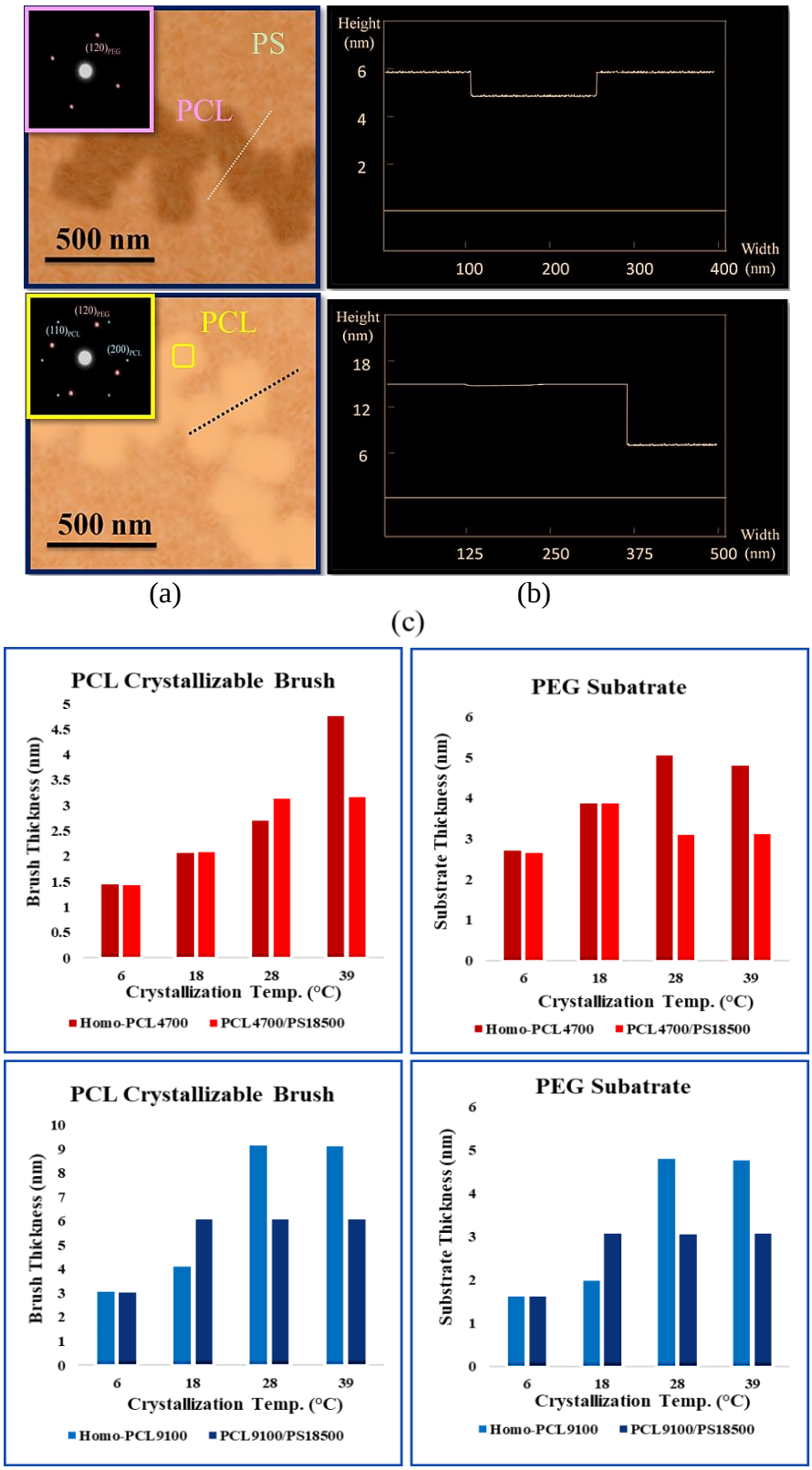

Fig. 3. AFM height images and the corresponding SAED patterns (a) as well as AFM height profiles (b) of PEG_{5000}-*b*-PS_{18500}/PEG_{5000}-*b*-PCL_{9100} single crystals grown at T_c= 6°C (top) and T_c= 39°C (bottom), in which the PCL brushes are amorphous and crystalline, respectively; the thickness trends of PCL brushes and PEG substrate via altering the crystallization temperature in PEG_{5000}-*b*-PCL and PEG_{5000}-*b*-PS_{18500}/PEG_{5000}-*b*-PCL single crystals (c).

[Downloaded from isee.iust.ac.ir on 2025-07-27]

[DOI: 10.22068/ijmse.2132]

In the PEG_{5000}-*b*-PS_{18500}/PEG_{5000}-*b*-$PLLA_{13300}$ mixed-brush single crystals, the $PLLA_{13300}$ brushes were crystallized at a lower temperature compared to the respective homo-brushes (18 versus 28°C) because of the induction effect of PS brushes on their crystallization (due to a repulsive interaction between the PS and PLLA brushes) [36]. The thickness of PEG substrate and PLLA brush crystals at T_c= 18°C were 3.76 and 10.65 nm, respectively. These characteristics were also retained at higher crystallization temperatures. The thickness of substrate and brush crystals at T_c= 28°C were 3.75 and 10.65 nm, and at T_c= 39°C were 3.71 and 10.67 nm, respectively. AFM height image, STEM image, and corresponding SAED pattern of PEG_{5000}-*b*-PS_{18500}/PEG_{5000}-*b*-$PLLA_{13300}$ single crystals formed at T_c= 18°C are shown in Figs. 4(a-c). The thickness trends of the PEG substrate and PCL brushes via changing the crystallization temperature are also depicted in Fig. 4(d) for the PEG_{5000}-*b*-PS_{18500}/PEG_{5000}-*b*-$PLLA_{13300}$ single crystals compared to the PEG_{5000}-*b*-$PLLA_{13300}$ ones.

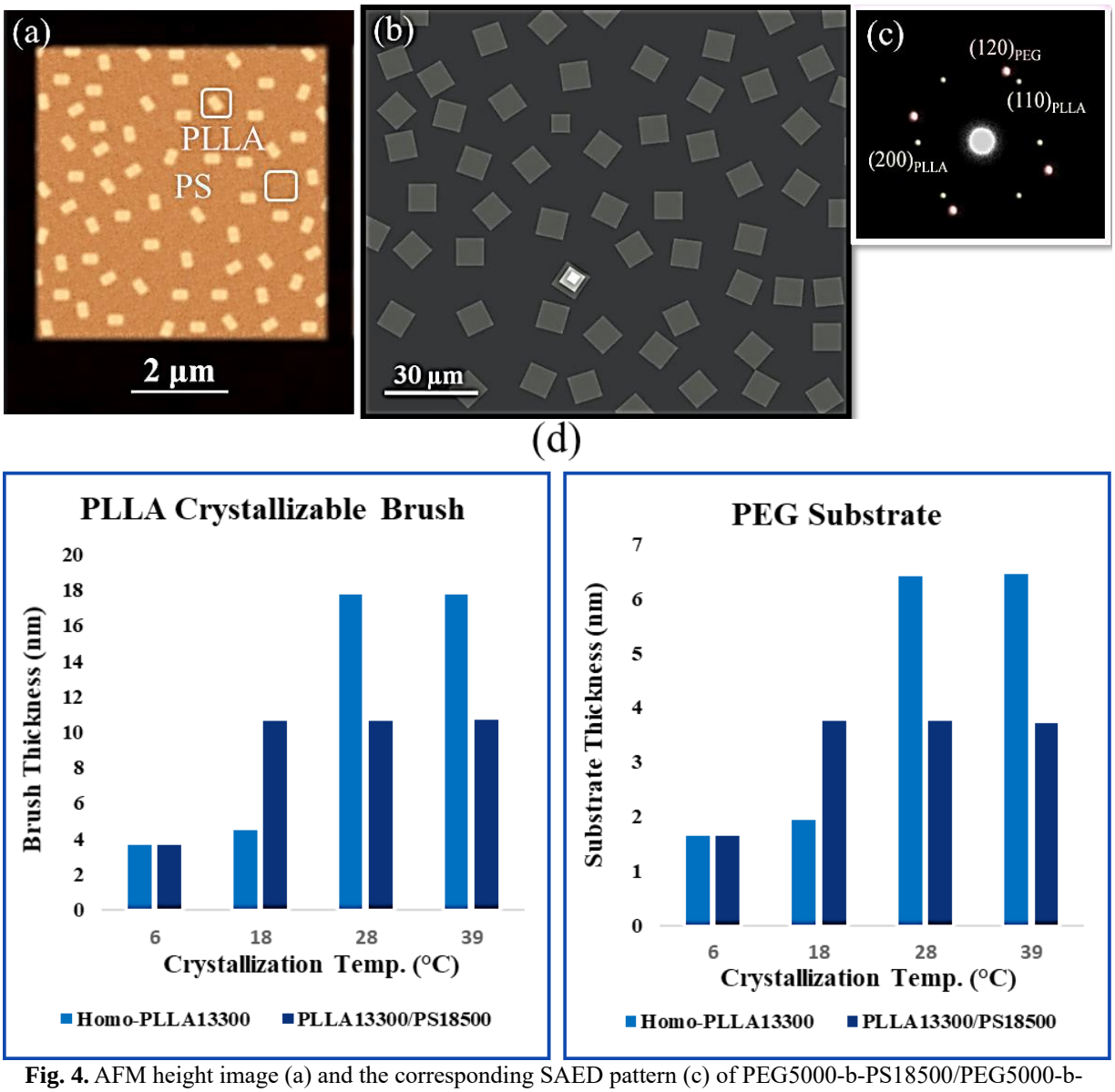

Fig. 4. AFM height image (a) and the corresponding SAED pattern (c) of PEG5000-b-PS18500/PEG5000-b-PLLA13300 single crystals grown at T_c= 18°C, in which the PLLA brushes are crystalline; STEM image of PEG5000-b-PS18500/PEG5000-b-PLLA13300 single crystals grown at T_c= 39°C (b); the thickness trends of PLLA brushes and PEG substrate via altering the crystallization temperature in PEG5000-b-PLLA13300 and PEG5000-b-PS18500/PEG5000-b-PLLA13300 single crystals (d).

[Downloaded from isee.iust.ac.ir on 2025-07-27]

[DOI: 10.22068/ijmse.2132]

For both PEG_{5000}-*b*-PS_{18500}/PEG_{5000}-*b*-PCL_{9100} and PEG_{5000}-*b*-PS_{18500}/PEG_{5000}-*b*-$PLLA_{13300}$ mixed-brush single crystals, via incorporation of crystallizable brushes into the crystalline structure, the substrate thickness increased compared to their amorphous state similar to the corresponding homo-brush systems. As above-mentioned, it could be attributed to the easier and higher rate of crystallization of the longer brushes compared to the osmotic pressure of their amorphous state on the substrate. Therefore, the PS brushes only caused the crystallizable brushes to nucleate easily and to crystallize at the lower temperatures; however, they did not change the crystallization rate and osmotic pressure ratio of crystallizable brushes because the osmotic pressure of brushes is less at the lower temperatures.

6. MIXED-BRUSHES COMPOSED OF PMMA AND CRYSTALLIZABLE BRUSHES

In the PEG_{5000}-*b*-$PMMA_{13100}$/PEG_{5000}-*b*-PCL_{4700} mixed-brush single crystals, the PCL_{4700} brushes were crystallized at 39°C, similar to their respective homo-brushes. As detected in previous systems, at each crystallization temperature in which the crystallization condition was provided, the single crystal characteristics remained constant even at the higher temperatures. By regarding this phenomenon and comparing the properties of given brushes in various systems, the nucleation commencement was focused. In more detail, in the above-mentioned mixed-brushes, the crystallization of PCL brushes was observed at a similar temperature for the corresponding homo-brushes. It could be deduced that the presence of PMMA brushes did not influence their crystallization. This was verified via comparing the features of PCL_{4700} brush single crystals in the mixed and homo-brush systems because the thickness of the substrate and brush single crystals in the mixed-brushes were 4.75 and 4.71 nm, and in the homo-brushes were 4.80 and 4.76 nm, respectively. The characteristics of brush crystals were similar in both homo- and mixed-brush systems thereby the nucleation occurred at a similar temperature, and the presence of PMMA brushes did not affect the crystallization. This could be originated from the low attractions between the PMMA and PCL brushes [37]. This phenomenon will be further discussed in the other systems in the upcoming sections. Figs. 5(a) and (b) display AFM height images and the corresponding SAED patterns of PEG_{5000}-*b*-$PMMA_{13100}$/PEG_{5000}-*b*-PCL_{4700} single crystals grown at 28 and 39°C, respectively. The thicknesses trends of PEG substrate and PCL brushes versus the crystallization temperature are also reported for the PEG_{5000}-*b*-$PMMA_{13100}$/ PEG_{5000}-*b*-PCL_{4700} single crystals in comparison to the PEG_{5000}-*b*-PCL_{4700} ones in Fig. 5(c). On the contrary, in PEG_{5000}-*b*-$PMMA_{13100}$/PEG_{5000}-*b*-$PLLA_{7800}$ and PEG_{5000}-*b*-$PMMA_{13100}$/PEG_{5000}-*b*-$PLLA_{13300}$ mixed-brush single crystals, the presence of PMMA brushes having a highly attractive interaction with the PLLA crystallizable grafts [38] hindered the crystallization of PLLA brushes. The PLLA brushes in these types of mixed-brushes were amorphous in a whole range of crystallization temperatures. In more detail, the high attraction between the PMMA and PLLA brush caused a low interaction between the crystallizable brushes and thereby prevented them from crystallization.

7. MIXED-BRUSHES DEVELOPED FROM VARIOUS CRYSTALLIZABLE BRUSHES IN THE VICINITY OF EACH OTHER

By the growth of PEG_{5000}-*b*-PCL_{4700}/PEG_{5000}-*b*-$PLLA_{7800}$, PEG_{5000}-*b*-PCL_{4700}/PEG_{5000}-*b*-$PLLA_{13300}$, and PEG_{5000}-*b*-PCL_{9100}/PEG_{5000}-*b*-$PLLA_{7800}$ single crystals, the mixed-brushes composed of double crystallizable brushes having distinct molecular weights were fabricated. In the mixed-brush single crystals in question, the presence of crystallizable brushes in the vicinity of each other did not alter their characteristics.

In the PEG_{5000}-*b*-PCL_{4700}/PEG_{5000}-*b*-$PLLA_{7800}$ mixed-brushes, the PCL_{4700} brushes were crystallized at T_c= 39°C, and the $PLLA_{7800}$ brushes were amorphous in a whole range of temperature, resembling their corresponding homo-brush systems. In the PEG_{5000}-*b*-PCL_{4700}/PEG_{5000}-*b*-$PLLA_{13300}$ mixed-brush single crystals, via enhancing the molecular weight of PLLA crystallizable brushes, the PCL_{4700} and $PLLA_{13300}$ brushes were crystallized at 39 and 28°C, respectively. Moreover, in the PEG_{5000}-*b*-PCL_{9100}/PEG_{5000}-*b*-$PLLA_{7800}$ mixed-brush systems, by increasing the molecular weight of

[Downloaded from isee.iust.ac.ir on 2025-07-27]

[DOI: 10.22068/ijmse.2132]

PCL crystallizable tethers, the PCL_{9100} brushes were crystallized at 28°C, and the $PLLA_{7800}$ brushes were amorphous in whole temperature range, exactly similar to their respective homo-brushes. It was obviously observed that in all these systems possessing any types of crystallizable brushes, the PCL_{4700}, PCL_{9100}, and $PLLA_{13300}$ brushes were crystallized at 39, 28, and 28°C, respectively, and the $PLLA_{7800}$ brushes were ever amorphous.

Fig. 6 displays AFM data and the corresponding SAED patterns of the PEG_{5000}-*b*-PCL_{4700}/PEG_{5000}-*b*-$PLLA_{7800}$ single crystals grown at T_c= 28°C (Figs. 6(a-d)) and the PEG_{5000}-*b*-PCL_{4700}/PEG_{5000}-*b*-$PLLA_{13300}$ single crystals prepared at T_c= 28°C and T_c= 39°C (Figs. 6(e-i)).

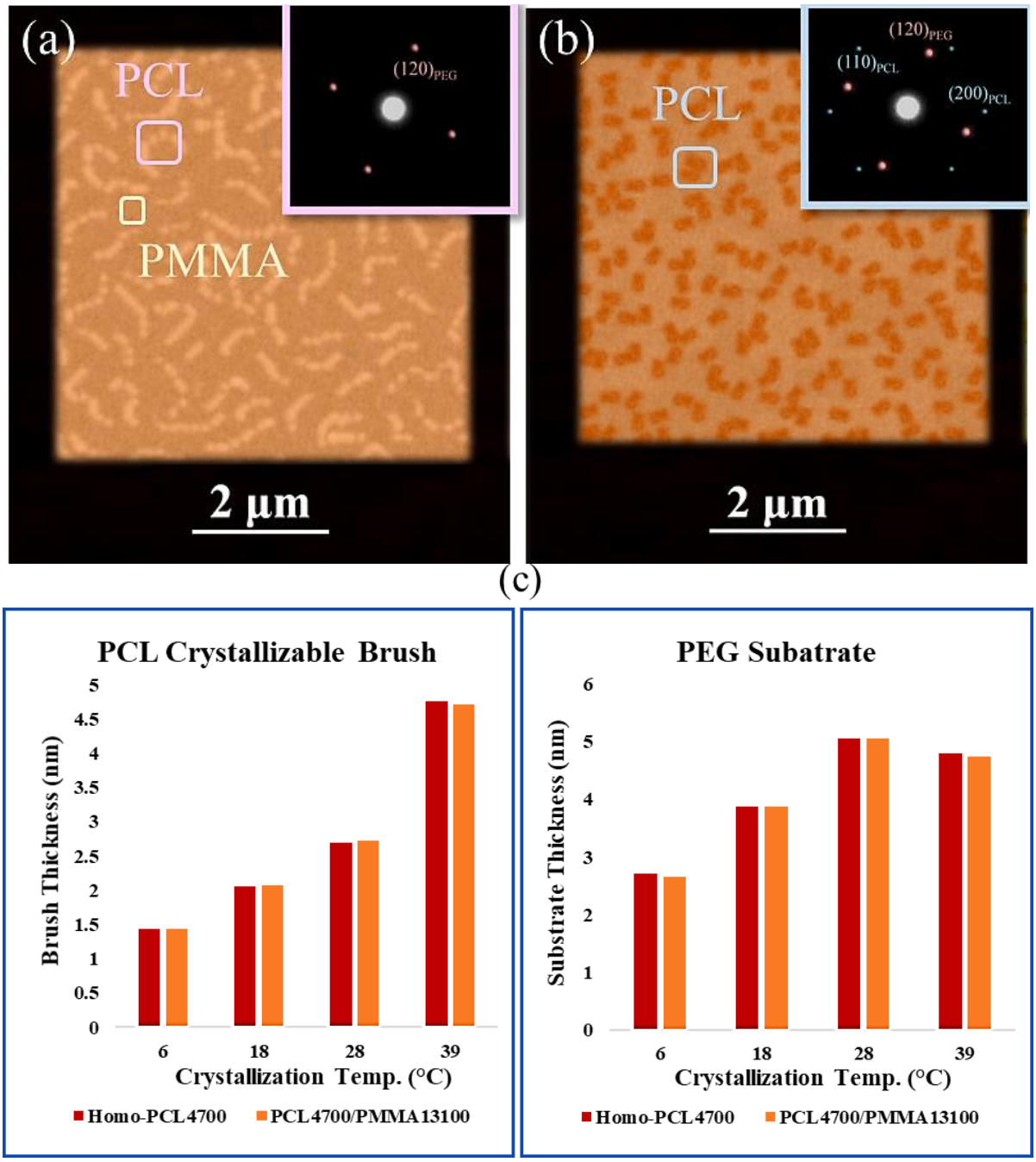

Fig. 5. AFM height images and the corresponding SAED patterns of PEG5000-b-PMMA13100/PEG5000-b-PCL4700 single crystals grown at T_c= 28°C (a) and T_c= 39°C (b), in which the PCL brushes are amorphous and crystalline, respectively; the thickness trends of PCL brushes and PEG substrate versus the crystallization temperature in PEG5000-b-PMMA13100/PEG5000-b-PCL4700 and PEG5000-b-PCL4700 single crystals (c).

[Downloaded from isee.iust.ac.ir on 2025-07-27]

[DOI: 10.22068/ijmse.2132]

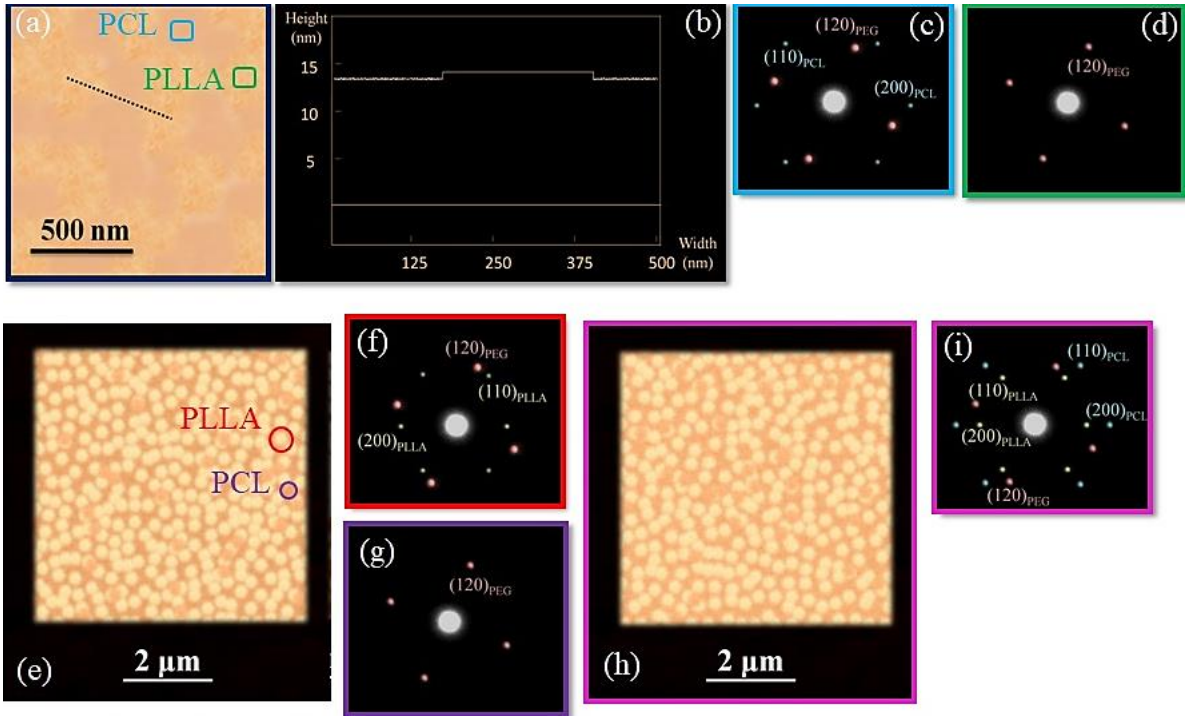

Fig. 6. AFM height image (a), AFM height profile (b) and the corresponding SAED patterns (c and d) of PEG5000-b-PCL4700/PEG5000-b-PLLA7800 single crystals grown at T_c= 39°C, in which PCL and PLLA brushes are crystalline and amorphous, respectively; AFM height image (e and h) and the corresponding SAED patterns (f and g) of PEG5000-b-PCL4700/PEG5000-b-PLLA13300 single crystals prepared at T_c= 28°C, in which PCL and PLLA brushes are crystalline and amorphous, respectively; the total ED pattern of PEG5000-b-PCL4700/PEG5000-b-PLLA13300 single crystals prepared at T_c= 39°C, in which PCL and PLLA tethers are crystalline (i).

Different parts of Fig. 7 also report the thickness trends of PEG substrate as well as PCL and PLLA brushes versus the crystallization temperature for the PEG_{5000}-*b*-PCL_{4700}/PEG_{5000}-*b*-$PLLA_{7800}$, PEG_{5000}-*b*-PCL_{9100}/PEG_{5000}-*b*-$PLLA_{7800}$, and PEG_{5000}-*b*-PCL_{4700}/PEG_{5000}-*b*-$PLLA_{13300}$ single crystals in comparison to their respective homo-brush systems.

To demonstrate the effectivity of neighboring brushes on the features in these systems, the homo- and mixed-brush single crystals were compared. For the PCL_{4700} brushes, the characteristics of the substrate and brush single crystals in the PEG_{5000}-*b*-PCL_{4700}/PEG_{5000}-*b*-$PLLA_{7800}$ and PEG_{5000}-*b*-PCL_{4700}/PEG_{5000}-*b*-$PLLA_{13300}$ mixed-brushes were 4.72, 4.70, 4.80, and 4.74 nm, respectively, and in the PEG_{5000}-*b*-PCL_{4700} homo-brushes were 4.80 and 4.76 nm, respectively. Hence, the nucleation occurred at a similar temperature and the presence of various crystallizable brushes in the vicinity of each other did not affect the crystallization strategy. Likewise, for the $PLLA_{13300}$ brushes, the properties of substrate and brush crystals in the PEG_{5000}-*b*-PCL_{4700}/PEG_{5000}-*b*-$PLLA_{13300}$ mixed-brushes were 6.42 and 17.71 nm, respectively, and in the PEG_{5000}-*b*-$PLLA_{13300}$ homo-brushes were 6.40 and 17.75 nm, respectively. The nucleation temperature in above-mentioned mixed- and homo-brush systems resembled each other. As another system, the characteristics of substrate and brush crystals of PCL_{9100} in the PEG_{5000}-*b*-PCL_{9100}/PEG_{5000}-*b*-$PLLA_{7800}$ mixed-brushes were 4.73 and 9.10 nm, respectively, and in the PEG_{5000}-*b*-PCL_{9100} homo-brushes were 4.80 and 9.13 nm, respectively. In these systems, the $PLLA_{7800}$ brushes were amorphous similar to their respective homo-brushes.

Furthermore, in all these single crystalline structures, the molecular weight of crystallizable brushes only affected the thickness of brush crystals and did not have any impact on the folding of crystallizable brushes and thus on the PEG substrate.

By large, the presence of crystallizable brushes in the vicinity of each other did not alter their

[Downloaded from isee.iust.ac.ir on 2025-07-27]

[DOI: 10.22068/ijmse.2132]

crystallization conditions, originating from a low attraction between them [39]. In fact, a weak attraction between the crystallizable brushes and their surrounding brushes did not affect their crystallization conditions. On the other hand, it was interesting that in these double crystallizable mixed-brush systems, even the crystallization of one type of brushes did not influence the crystallization of other type. This may be related to the ordered configuration of developed crystallites on the PEG substrate.

8. MIXED-BRUSHES OF CRYSTALLIZABLE BRUSHES NEIGHBORING THE PANI NANORODS

In this section, the mixed-brush single crystals of PEG_{5000}-*b*-$PANI_{3120}$/PEG_{5000}-*b*-PCL_{4700}, PEG_{5000}-*b*-$PANI_{3120}$/PEG_{5000}-*b*-PCL_{9100}, PEG_{5000}-*b*-$PANI_{3120}$/PEG_{5000}-*b*-$PLLA_{7800}$ and PEG_{5000}-*b*-$PANI_{3120}$/PEG_{5000}-*b*-$PLLA_{13300}$ were developed.

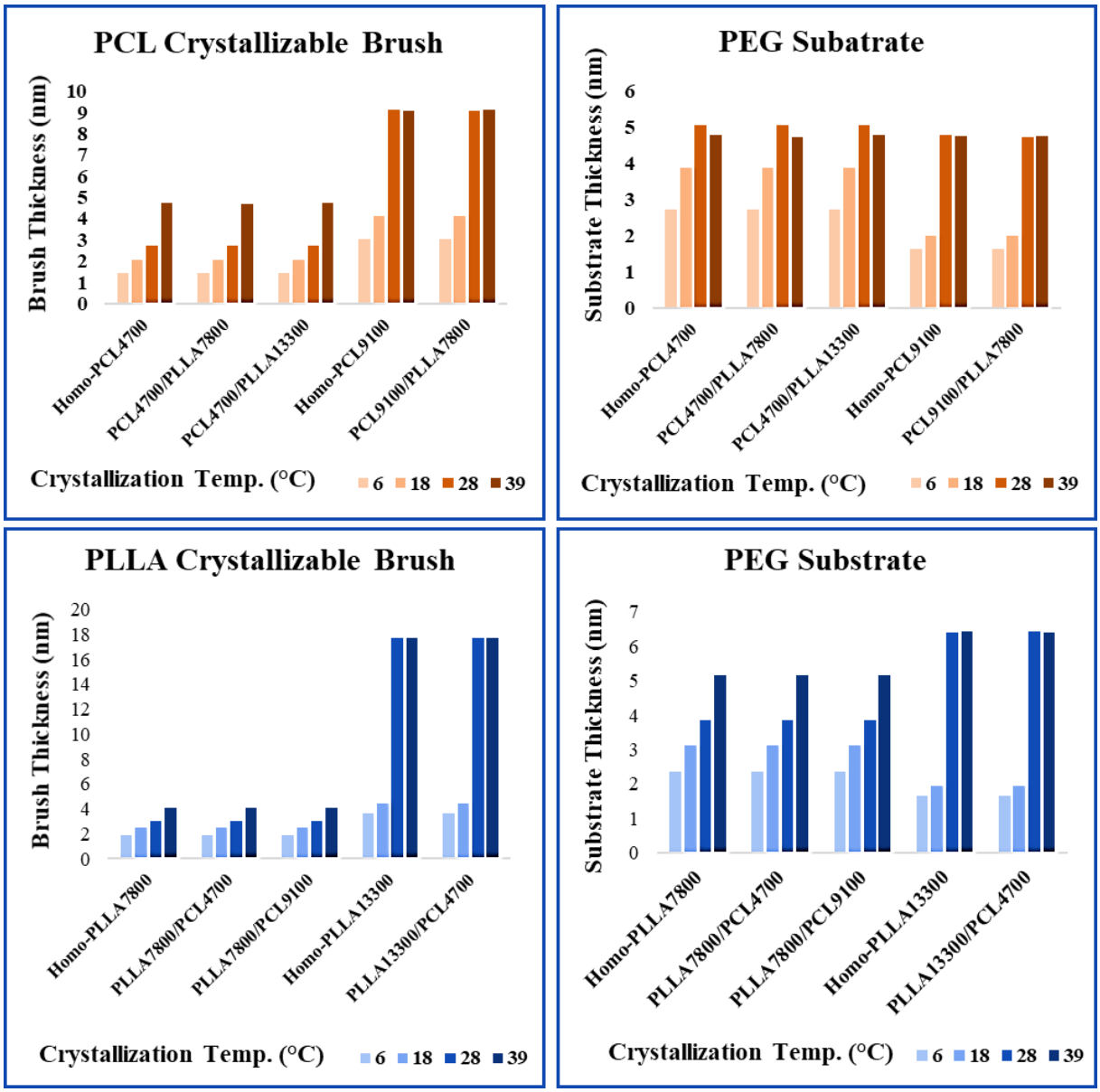

Fig. 7. Thickness trends of PEG substrate as well as the PCL and PLLA brushes versus the crystallization temperature in PEG5000-b-PCL4700/PEG5000-b-PLLA7800, PEG5000-b-PCL9100/PEG5000-b-PLLA7800, and PEG5000-b-PCL4700/PEG5000-b-PLLA13300 single crystals compared to their respective homo-crystallizable brushes.

[Downloaded from isee.iust.ac.ir on 2025-07-27]

[DOI: 10.22068/ijmse.2132]

The presence of PANI nanorods in the vicinity of crystallizable brushes highly induced the crystallization, and even the short brushes of PCL_{4700} and $PLLA_{7800}$ were crystallized at the lower temperatures (i.e., 18°C). Thanks to a strong crystallization induction and crystallization commencement at the lower temperatures, the thickness of brush and substrate crystals were lower than those detected for previous systems.The characteristics of substrate and brush crystals of PCL_{4700}, PCL_{9100}, $PLLA_{7800}$ and $PLLA_{13300}$ grafts at 18°C were 2.28, 2.36, 2.25, 4.55, 2.61, 4.45, 2.61 and 7.60 nm, respectively. Figs. 8(a-c) represent the AFM height images and the corresponding SAED patterns of PEG_{5000}-*b*-PCL_{4700}/PEG_{5000}-*b*-$PANI_{3120}$ single crystals grown at T_c= 18°C and PEG_{5000}-*b*-$PLLA_{7800}$/PEG_{5000}-*b*-$PANI_{3120}$ prepared at T_c= 18°C as well as the thickness trends of PEG substrate and the PCL/PLLA brushes with respect to the crystallization temperature. In the case of PCL_{4700} brushes similar to the corresponding previous systems, through incorporation of brushes into the single crystalline structure, their thickness increased; however, the substrate thickness decreased. On the other hand, in the PEG_{5000}-*b*-$PANI_{3120}$/ PEG_{5000}-*b*-$PLLA_{7800}$ mixed-brush nanostructures, via entering the $PLLA_{7800}$ brushes into the single crystalline structure, the brush thickness increased, whereas the substrate thickness decreased compared to their corresponding amorphous state. It could be assigned to the difficulty of crystallization of short $PLLA_{7800}$ tethered chains, which resulted in a slow crystallization. The folding numbers of brush crystals increased and, consequently, the PEG substrate thickness was justified to reach a desired condition. The consequence was an enhancement in the substrate folding and thus a lower thickness. On the other hand, it was obviously observed that in these systems via elevating the molecular weight of crystallizable brushes, just the thickness of brush crystal increased and the properties of substrate and brush single crystals remained constant at the higher crystallization temperatures. The presence of rigid PANI nanorods only caused an easier crystallization within a shorter time. By respecting the extended lengths of PCL_{4700} (35.15 nm), PCL_{9100} (68.05 nm), $PLLA_{7800}$ (31.2 nm) and $PLLA_{13300}$ (53.2 nm) and the thickness of brush crystals (2.35, 4.55, 4.45 and 7.60 nm, respectively) which were constant at higher temperature, the folding numbers were around 15, 15, 7 and 7, respectively. Therefore, even the strong induction of PANI nanofibers did not affect the ratio of crystallization rate and osmotic pressure for the crystallizable brushes as well. It means that the substrate thickness for the crystallized PCL_{4700} and $PLLA_{7800}$ decreased and for the PCL_{9100} and $PLLA_{13300}$ ones increased.

In conclusion, in the mixed-brush systems having the PANI nanorods, due to a strong crystallization induction, the lowest nucleation temperatures were detected. The PS brushes with a mediocre crystallization induction demonstrated the higher nucleation temperatures compared to the PANI-based systems. The mixed-brushes with the PMMA and double crystalline brushes behaved like the crystallizable homo-brush samples, and their nucleation temperatures were higher than the two previous systems. Finally, the PMMA brushes completely hindered the crystallization of PLLA grafts. The induction effect of neighboring brushes did not influence the crystallization rate and osmotic pressure ratio of crystallizable brushes and only provided easier nucleation for them.

In all designed homo- and mixed-brush nanostructures, an enhancement in the molecular weight of crystallizable brushes only facilitated the crystallization of one end-restricted brush and had no effect on the crystal folding number. Moreover, via elevating the crystallization temperature, all aspects of brush and thus substrate single crystals remained constant. Hence, the novel biocompatible nanostructures with a three-layer fully single crystalline state were obtained and retained even at higher temperatures. On the other hand, by entering the short crystallizable chains to the crystalline state, their thickness increased, and simultaneously the substrate thickness decreased. In contrast, in the long crystallizable brushes, the incorporation of brushes into a single crystalline structure reflected a lower brush crystal thickness and simultaneously a higher substrate thickness, compared to that detected for the corresponding amorphous brushes. As another point, the neighboring brushes just affected the hindrance or the nucleation commencement of crystallization for the crystallizable brushes and had no influence on the crystallization properties of single crystals.

[Downloaded from isee.iust.ac.ir on 2025-07-27]

[DOI: 10.22068/ijmse.2132]

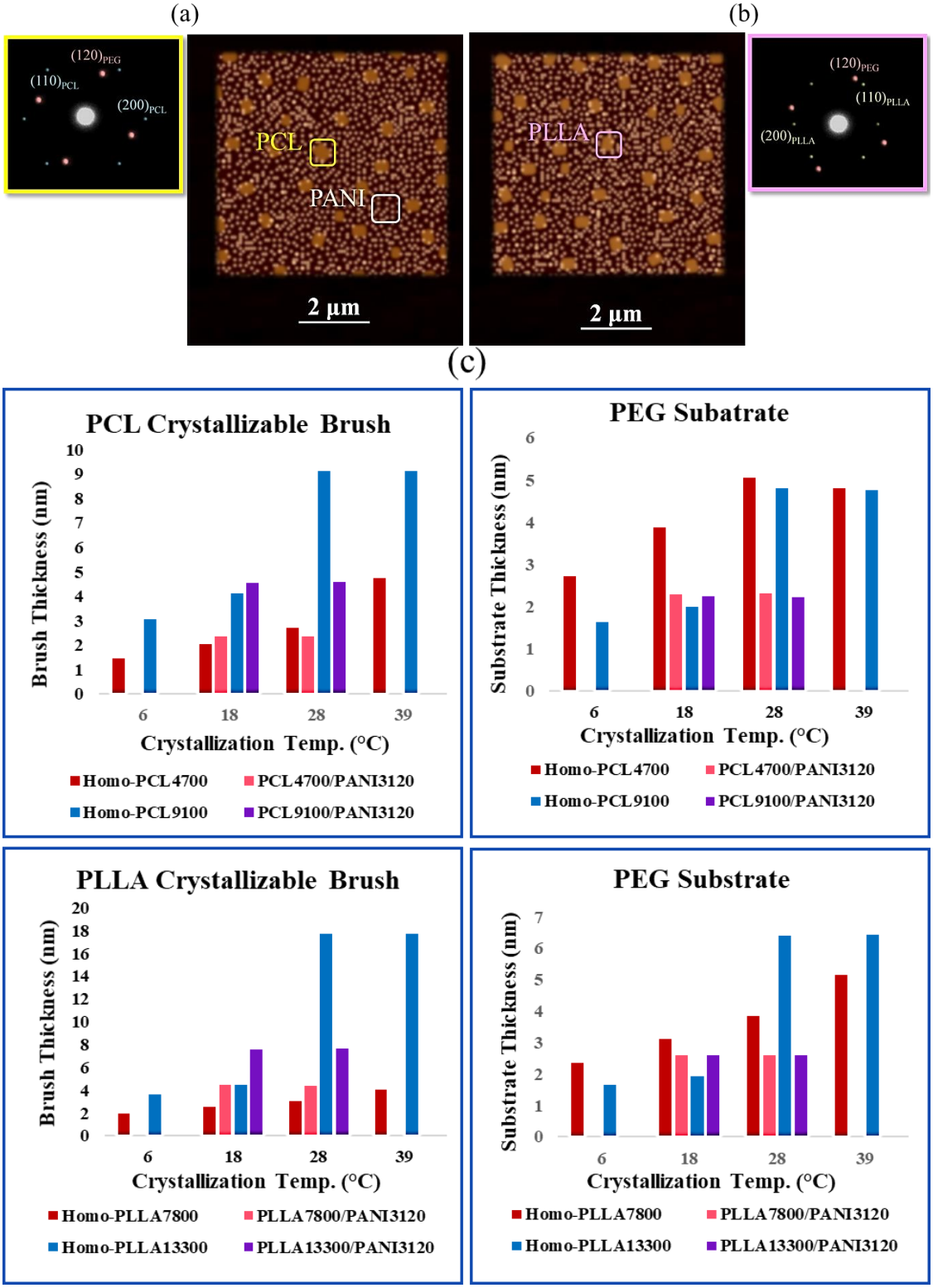

Fig. 8. AFM height images and the corresponding SAED patterns of PEG5000-b-PCL4700/PEG5000-b-PANI3120 single crystals grown at T_c= 18°C (a) and PEG5000-b-PLLA7800/PEG5000-b-PANI3120 single crystals prepared at T_c= 39°C (b), in which the PCL and PLLA brushes are crystalline; the thickness trends of PEG substrate and PCL/PLLA brushes versus the crystallization temperature in PEG5000-b-PCL4700/PEG5000-b-PANI3120, PEG5000-b-PANI3120/PEG5000-b-PCL9100, PEG5000-b-PLLA7800/PEG5000-b-PANI3120, and PEG5000-b-PANI3120/PEG5000-b-PLLA13300 mixed-brush single crystals compared to their corresponding homo-crystallizable brushes (c).

[Downloaded from isee.iust.ac.ir on 2025-07-27]

[DOI: 10.22068/ijmse.2132]

Fig. 9 schematically illustrates the variations in the single crystal specifications with respect to the molecular weight and crystallization temperature in various systems.

The interface distribution function (IDF) of SAXS for the PEG_{5000}-*b*-PCL_{9100} single crystals at T_c= 28°C, PEG_{5000}-*b*-PCL_{4700}/PEG_{5000}-*b*-PS_{18500} single crystals at T_c= 18°C, PEG_{5000}-*b*-PCL_{4700}/PEG_{5000}-*b*-$PLLA_{13300}$ single crystals at T_c= 28°C, and PEG_{5000}-*b*-$PANI_{3120}$/PEG_{5000}-*b*-$PLLA_{7800}$ single crystals at T_c= 18°C are illustrated in Figs. 10 (a–d), respectively. More details of SAXS profiles are reported in Supplementary Information. In the IDF of homo-brush systems such as PEG_{5000}-*b*-PCL_{9100} single crystals (Fig. 10(a)), the first and second peaks demonstrated the PEG substrate (= 4.80 nm) and twice of PCL brushes (= 18.26 nm) thicknesses, respectively. The valley was for the overall thickness of grown single-crystal (= 23.10 nm). In the SAXS profiles of mixed-brush single crystals, the first to fourth peaks stood for the thicknesses of crystalline PEG substrate beneath various brushes and twice of the thicknesses of grafted brushes. As an instance, in the IDF of Fig. 10(c) detected for the PEG_{5000}-*b*-PCL_{4700}/PEG_{5000}-*b*-$PLLA_{13300}$ single crystals grown at 28°C, the four peaks from left demonstrate 5.05, 5.48, 6.42, and 35.40 nm for the thicknesses of PEG substrate beneath the PCL brushes, twice of the height of PCL grafts, PEG substrate underneath the PLLA brushes and twice of the height of PLLA crystal, respectively. The 2-fold values for the thicknesses of polymer brushes were originated from the sandwiched structure of grown single crystals. STEM images and DSC data of some samples are provided in Supplementary information.

9. CONCLUSIONS

In this work, the crystallization behavior of crystallizable PCL and PLLA brushes were studied in the homo- and mixed-brushes through designing the PEG-*b*-PCL and PEG-*b*-PLLA single crystals from dilute solution. To this purpose, the single crystals sandwiched between the crystallizable PCL and PLLA brushes using distinct copolymers including the blocks of PEG, PCL, PLLA, PS, PMMA, and PANI were designed and employed to study the effective parameters. The crystallization circumstance of PEG substrate and PCL/PLLA brushes, as well as their effects on the crystallization, were focused. The chemical environment was investigated through the interactions of crystallizable brushes with the surrounding brushes. In addition, the physical environment was covered by the amorphism/crystallinity and rigidity/flexibility of neighboring brushes.

Conflicts of interest. There are no conflicts of interest to declare.

Funding. There is no funding for this work.

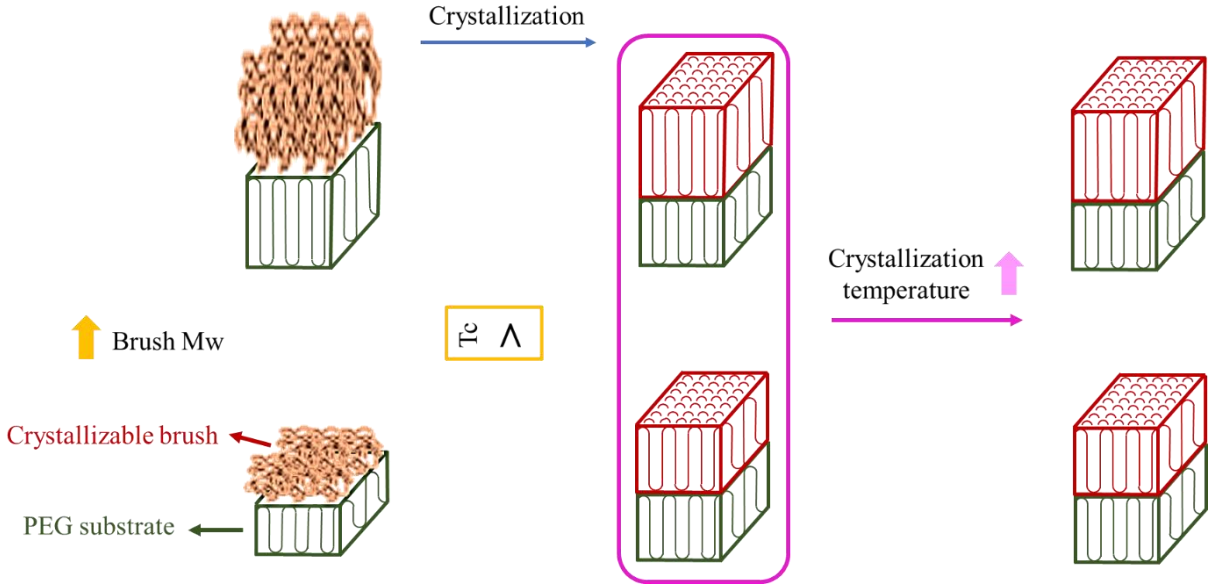

Fig. 9. Scheme of single crystallization behavior of crystalline-crystalline block copolymers through changing the molecular weight of crystallizable brushes and crystallization temperature.

[Downloaded from isee.iust.ac.ir on 2025-07-27]

[DOI: 10.22068/ijmse.2132]

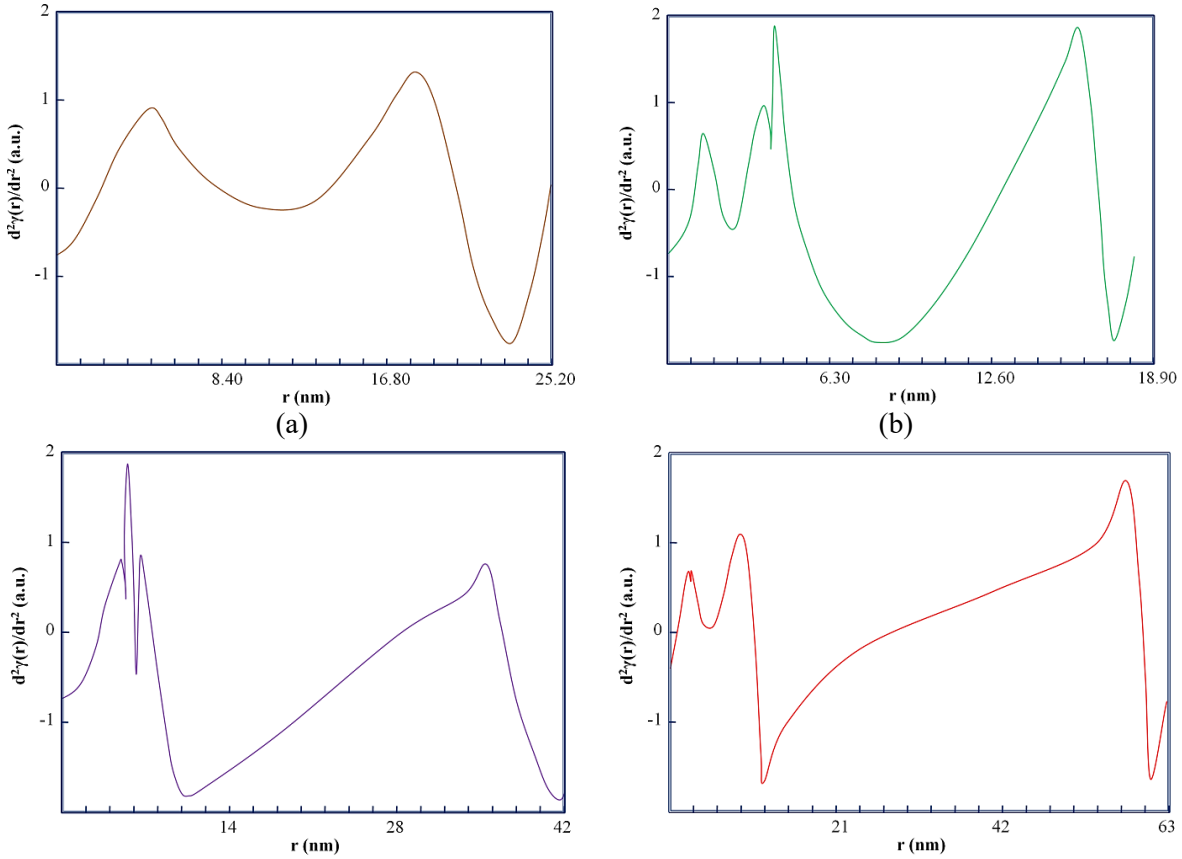

Fig. 10. IDF of SAXS of PEG5000-b-PCL9100 single crystals grown at T_c= 28°C (a); PEG5000-b-PCL4700/PEG5000-b-PS18500 single crystals grown at T_c= 18°C (b); PEG5000-b-PCL4700/PEG5000-b-PLLA13300 single crystals grown at T_c= 28°C (c); PEG5000-b-PANI3120/PEG5000-b-PLLA7800 single crystals grown at T_c= 18°C (d).

10. APPARATUS

10.1. Atomic force microscopy

To measure the overall single crystal thickness and identify their surface morphologies, the single crystals were observed under an atomic force microscope (AFM, Nanoscope IIIA). The height and phase images helped investigate the surface topologies of tethered chains on the PEG lamellar substrate. The single crystal dispersion was dropped onto a silicon wafer and quickly dried by a stream of high purity nitrogen and observed under AFM. A silicon tip in the tapping mode was utilized. During AFM scanning, the cantilever tip-to-sample force required to be carefully adjusted to avoid damages. For the tip-to-sample force, a large force could lead to tip penetrations into the thin tethered chain layers, and disturb the materials at the layer surfaces. A scan rate of 1 Hz and a resolution of 512 × 512 were selected to take high quality images.

Transmission electron microscopy: The structure and morphology of grown single crystals were identified using a transmission electron microscope (Philips CM30 TEM) with an accelerating voltage of 100 KeV. The selected area electron diffraction (SAED) experiments were also conducted to determine the chain orientation in the single crystals.

Scanning transmission electron microscopy: Scanning transmission electron microscopy (STEM) experiments were carried out adopting a FEI Quanta 400 operated at 30 kV with a tungsten filament.

Small angle X-ray scattering: The characteristics of single crystals were also verified by the small angle X-ray scattering (CMOS flat panel SAXS detector (C9728DK)) measurements with a counts rate of 1000 s/s/channel. The structure of the single crystals could be investigated using the

[Downloaded from isee.iust.ac.ir on 2025-07-27]

[DOI: 10.22068/ijmse.2132]

interface distribution function (IDF) of SAXS. The IDF ($g_1(r)$), which provided a series of the distance distributions with alternating signs, was calculated by the second derivative of the 1D electron density correlation function. This function was correlated to the scattering intensity by a Fourier transform. The SAXS intensities were detected from the single crystal mats in the dry state. The correlation and interference distribution functions allowed determining the lamellar stacking periodicity and discriminate the crystalline and non-crystalline and double crystalline layers. More details are represented below.

Calculation and analysis of the 1D correlation function $\gamma_1(r)$: The one dimensional (1D) electron density correlation function $\gamma_1(r)$ is related to the scattering intensity by a Fourier transform. However, several corrections are necessary before proceeding with Fourier operation. Since the intensity curve is collected over a finite range of s values, the curves may require extrapolation on both sides of the s-interval. The extrapolation to zero s-value can be performed using Debye-Bueche model [1] as follows:

$$I(s) = \frac{C}{(1 + 4\pi^2\xi^2 s^2)^2} \quad (1)$$

In Equation (1), C is a constant and ξ is the inhomogeneity length. C and ξ can be determined from the plot of $I(s)^{-0.5}$ versus s^2 using the intensity data in the low s-region. Some other options of acquisition of the low s-value have included linear or polynomial extrapolations of this part of the SAXS curve. In the case where the interface between the two layers is not sharp, the extension of intensity to large s-values is accomplished according to Porod–Ruland [2] model:

$$\lim_{s\to\infty} I(s) = \frac{K_p}{s^4} e^{-4\pi^2 s^2 \sigma^2} \quad (2)$$

In Equation (2), the exponential term accounts for the presence of the crystal/amorphous interface (σ is related to the thickness of the transition layer between crystalline and amorphous regions in lamellar stacks). The data was fitted in the range $0.01 \leq s \leq 0.03$ Å^{-1} with Equation (2), substituted by the fitting results and extrapolated to $s = 0.1$ Å^{-1} after subtracting the constant background B. The background is the result of the density fluctuation, leading to a departure from linearity as depicted from Porod's law, and should be corrected with a function of the form:

$$B = a + bs^n$$

$$B = ae^{-bs^2} \quad (3)$$

In Equation (3), a,b and n are constants.

The fully corrected intensity $I_C(s)$ was used to compute the one-dimensional correlation function corresponding to the electron density fluctuations perpendicular to the lamellar basal plane [3]:

$$\gamma_1(r) = \frac{\int_0^\infty I_c(s)s^2 \cos(2\pi rs)\, ds}{\int_0^\infty I_c(s)s^2 ds} \quad (4)$$

In the other words, the electron density correlation function is obtained from the real part of Fourier transform of the fully corrected intensity. The choice of the value for Lorenz correction will be discussed later. The final form for the computation of the correlation function is as follows:

$$\gamma_1(r) = Re\left\{\int_0^\infty (I_c(s) - B)s^n e^{(2\pi isr + 4\pi^2 s^2\sigma^2)} ds\right\} \quad (5)$$

The correlation function is normalized to unity at the origin.

Fig. S1(a) displays the micro-structural parameters that can be obtained from the 1D correlation function. This interpretation assumes that the sample has an ideal lamellar morphology. The 1D correlation function approach, following the original contribution of Vonk and Kortleve [3], was designed for homogeneous ideal two-phase systems where a series of triangles centered at r= 0, LB (total thickness), 2LB, etc., reflect correlations of the lamella with its next neighbors, second neighbors, etc. The horizontal line that passes through the bases of the triangles is called the baseline. The determinations of LB, substrate thickness (L_c), amorphous or crystalline brush thickness (L_a), and ratio of ordering (Φ_L) may be realized by locating the first minimum and maximum in the correlation function. The long period of L_P or LB referred to as the Bragg peak, is estimated from the position of the first maximum of $\gamma_1(r)$. On the other hand, the negative ordinate, γ_{min}, is related to crystallinity Φ_L, as follows:

[Downloaded from isee.iust.ac.ir on 2025-07-27]

[DOI: 10.22068/ijmse.2132]

$$\gamma_{min} = \frac{-\emptyset_l}{1-\emptyset_l} \quad (6)$$

So, the first minimum of the 1D correlation function can be used to determine the value of Φ_L. The lamellar and amorphous layer thicknesses can then be calculated for example as:

$$Lc = \emptyset_l LB, \qquad La = (1-\emptyset_l)LB \quad (7)$$

Calculation and analysis of the interface distribution function approach. Further details of the micro-structure of the two-phase system can be analyzed using the IDF developed by Ruland [4]. The IDF provides a series of the distance distributions with alternating signs, which are composed together (Fig. S1(b)). The interface distribution function, denoted in this manuscript as $g_1(r)$, can be calculated by two different ways:

1) by the second derivative of the 1D correlation function $\gamma_1(r)$:

$$g_1(r) = \frac{\delta^2(\gamma_1(r))}{\delta r^2} = \gamma_1''(r) \quad (8)$$

2) as a Fourier transform of the interference function $G_1(r)$ which is Fourier transform of the scattering intensity after subtraction of the Porod law:

$$g_1(r) = \int_{-\infty}^{+\infty} G(s)\cos(sr)\,ds \quad (9)$$

This IDF represents the probability distribution of finding two interfaces separated by a distance r. The values of the IDF are negative if the two phases are the same and vice versa. As shown by Stribeck and Ruland [5] from the analysis of this function one can obtain LB, L_c, L_a and the width of the corresponding distributions.

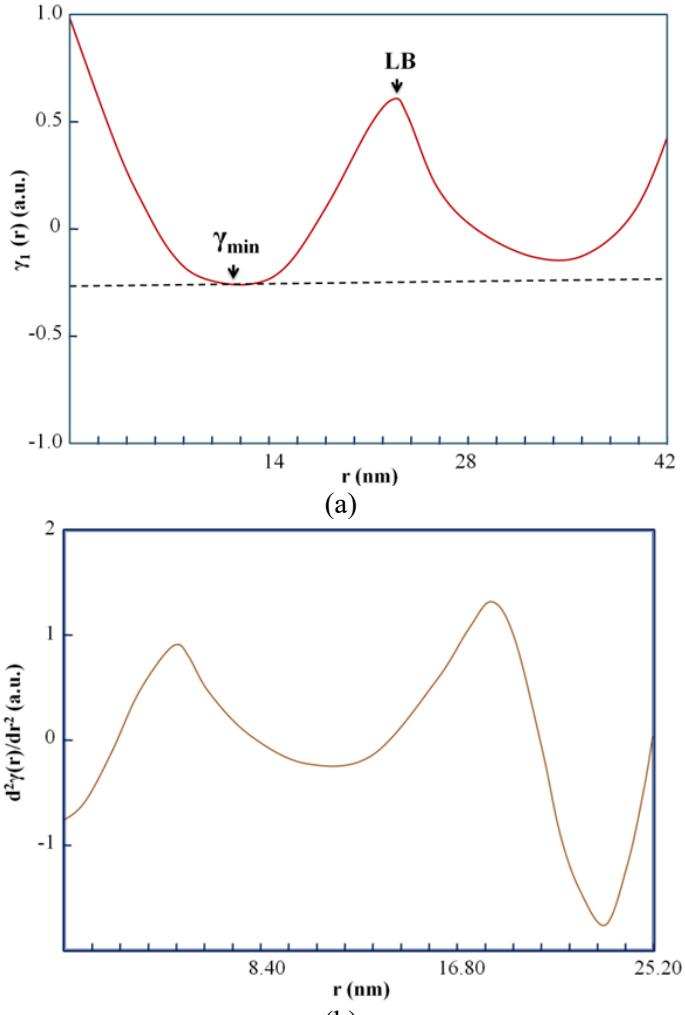

Fig. S1. 1D correlation function ($\gamma_1(r)$) (a) and of IDF (b) of SAXS of PEG5000-b-PCL9100 single crystals grown at T_c= 28°C.

[Downloaded from isee.iust.ac.ir on 2025-07-27]

[DOI: 10.22068/ijmse.2132]

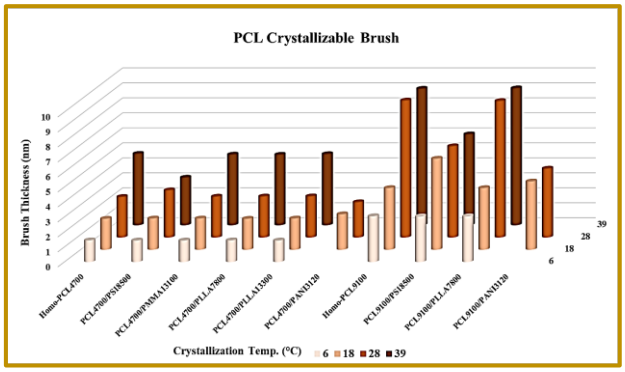

(a)

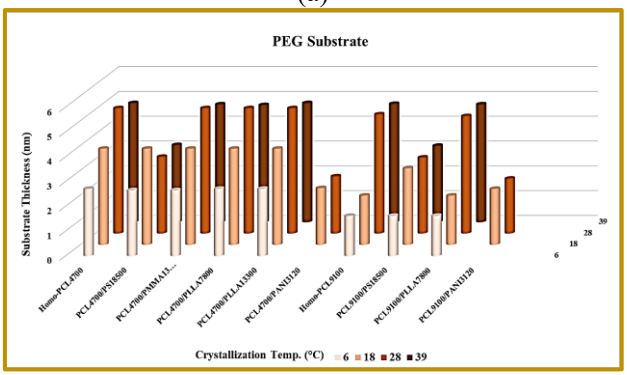

(b)

Fig. S2. PCL brush (a) and PEG substrate (b) thickness variation trend with respect to the crystallization temperature in various single crystal systems.

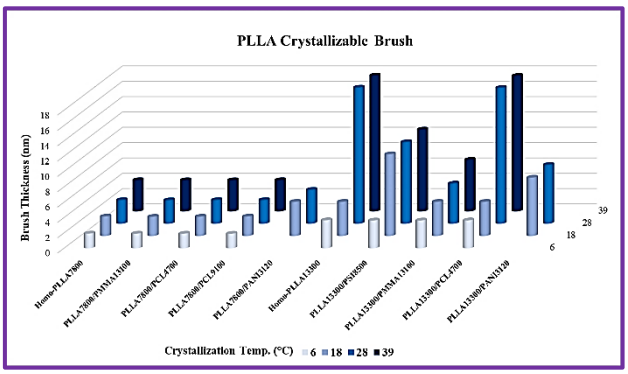

(a)

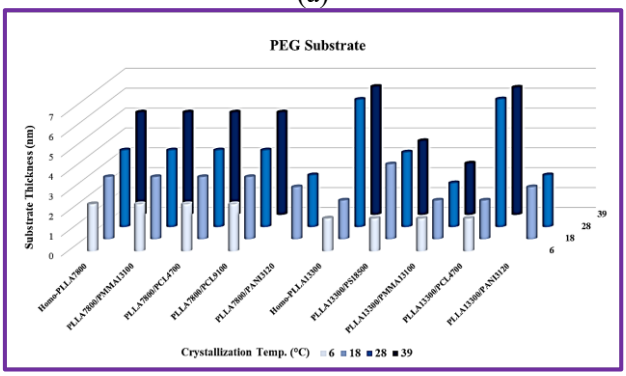

(b)

Fig. S3. PLLA brush (a) and PEG substrate (b) thickness variation trend with respect to the crystallization temperature in various single crystal systems.

[Downloaded from isee.iust.ac.ir on 2025-07-27]

[DOI: 10.22068/ijmse.2132]

Scanning transmission electron microscopy (STEM):

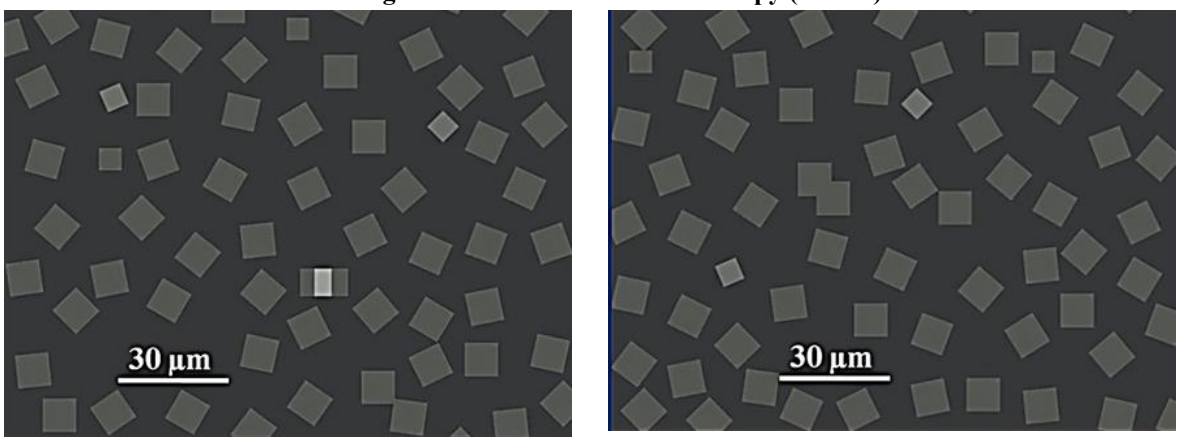

(a) (b)

Fig. S4. STEM images of PEG5000-b-PANI3120/PEG5000-b-PLLA13300 single crystals grown at T_c= 28°C (a) and PEG5000-b-PLLA13300 single crystals grown at T_c= 28°C (b).

Differential scanning calorimetry (DSC):

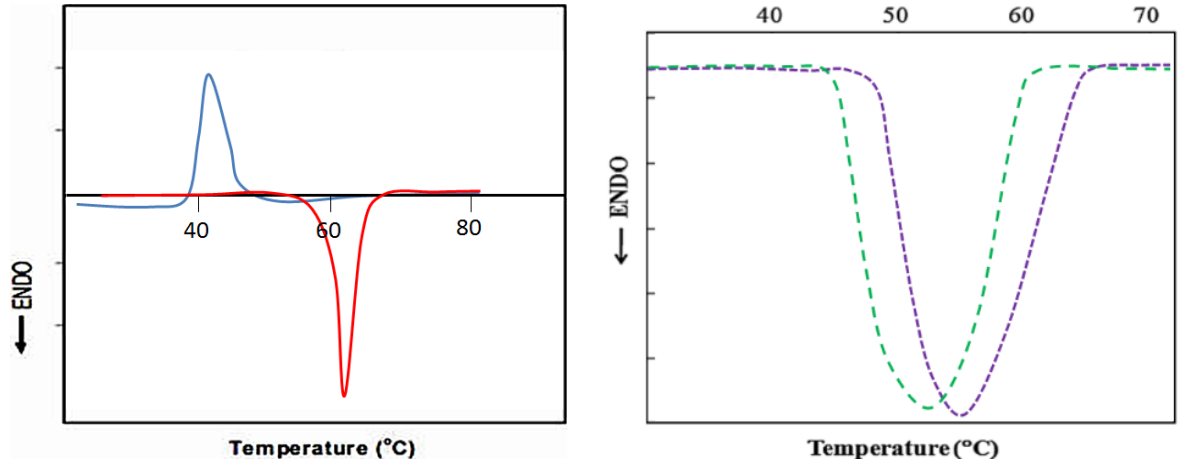

(a) **(b)**

Fig. S5. DSC heating and cooling cycles with the scanning rate of 5 K/min for the collected mats of PEG-b-PCL single crystals (a) (T_c= 41°C and T_m= 61°C); heating cycle with the scanning rate of 5 K/min for collected mats of PEG-b-PLLA single crystals (T_m= 55°C) and for the bulk of PEG-b-PLLA diblock copolymers (T_m= 52°C) (b).

REFERENCES

[1] Van Horn, R. M.; Steffen, M. R.; O'Connor, D. Recent Progress in Block Copolymer Crystallization. Polym. Cryst. 2018, 1, e10039.

[2] Palacios, J. K.; Mugica, A.; Zubitur, M.; Müller, A. J.; Crystallization in Multiphase Polymer Systems. 2018, p. 123.

[3] Agbolaghi, S.; Abbaspoor, S.; Abbasi, F. A Comprehensive Review on Polymer Single Crystals— From Fundamental Concepts to Applications. Prog. Polym. Sci. 2018, 81, 22–79.

[4] Abbaspoor, S.; Agbolaghi, S.; Mahmoudi, M.; Jahanbani, Y.; Abbasi, F.; Sarvari, R. Effect of miscibility on migration of third component in star-like co-continuous and disperse-within-disperse mixed brushes. Polym. Int. 2018, 67, 141–150.

[5] Abbaspoor, S.; Agbolaghi, S; Abbasi, F. Chemical and Physical Effects of Processing Environment on Simultaneous Single Crystallization of Biodegradable Poly(ε-caprolactone) and Poly(l-lactide) Brushes and Poly(ethylene glycol) Substrate. Eur. Polym. J. 2018, 103, 293–303.

[Downloaded from isee.iust.ac.ir on 2025-07-27]

[DOI: 10.22068/ijmse.2132]

[6] Sun, J.; Chen, X.; He, C.; Jing, X. Morphology and Structure of Single Crystals of Poly(ethylene glycol)-Poly(ε-caprolactone) Diblock Copolymers. Macromolecules 2006, 39, 3717−3719.

[7] Jiang, N.; Jiang, S.; Hou, Y.; Yan, S.; Zhang, G.; Gan, Z. Influence of Chemical Structure on Enzymatic Degradation of Single Crystals of PCL-b-PEO Amphiphilic Block Copolymer. Polymer 2010, 51, 2426–2434.

[8] Van Horn, R. M.; Zheng, J. X.; Sun, H-J.; Hsiao, M-S.; Zhang, W-B.; Dong, X-H.; Xu, J.; Thomas, E. L.; Lotz, B.; Cheng, S. Z. D. Solution Crystallization Behavior of Crystalline− Crystalline Diblock Copolymers of Poly(ethylene oxide)-block-Poly(ε-caprolactone). Macromolecules 2010, 43, 6113−6119.

[9] Sun, J.; He, C.; Zhuang, X.; Jing, X.; Chen, X. The Crystallization Behavior of Poly(ethylene glycol)- Poly(ε-caprolactone) Diblock Copolymers with Asymmetric Block Compositions. J. Polym. Res. 2011, 18, 2161−2168.

[10] Abbaspoor, S.; Agbolaghi, S.; Nazari, M.; Abbasi, F. Conventional and rare-patched rod/coil matrix-dispersed patternings on single crystals affected by Rigidity, amorphism and crystallinity of brushes. Eur. Polym. J. 2017, 94, 446−459.

[11] Ridolfo, R.; Arends, J.J.; van Hest, J.C.; Williams, D.S., Wormlike Nanovector with Enhanced Drug Loading using Blends of Biodegradable Block Copolymers. Biomacromolecules 2020, 21, 2199−2207.

[12] Hoang Thi, T. T., Sinh, L. H., Huynh, D. P., Nguyen, D. H., & Huynh, C. (2020). Self-Assemblable Polymer Smart-Blocks for Temperature-Induced Injectable Hydrogel in Biomedical Applications. Front. Chem. 2020, 8, 19.

[13] Lin, X., Wang, X., Tian, H. Oral delivery of WR-1065 by ROS-responsive PEG-PCL Nanoparticles for Radioprotection. Colloid. Surface. A. 2020, 599, 124886.

[14] Ali, I.; Kareem, F.; Rahim, S.; Perveen, S.; Ahmed, S.; Shah, M. R.; Malik, M. I. Architecture Based Selectivity of Amphiphilic Block Copolymers of Poly(ethylene oxide) and Poly(ε-caprolactone) for Drug Delivery. Reactive and Functional Polymers, 2020, 150, 104553.

[15] Casalini, T.; Rossi, F.; Castrovinci, A.; Perale, G. (2019). A Perspective on Polylactic Acid-Based Polymers Use for Nanoparticles Synthesis and Applications. Front. Bioeng. Biotech. 2019, 7, 259.

[16] Chen, L., Wang, S., Yu, Q., Topham, P. D., Chen, C., & Wang, L. (2019). A Comprehensive Review of Electrospinning Block Copolymers. Soft Matter, 2019, 15, 2490-2510.

[17] Wang, J.; Li, S.; Han, Y.; Guan, J.; Chung, S.; Wang, C.; Li, D. (2018). Poly(Ethylene Glycol)– polylactide micelles for cancer therapy. Front. pharmacol. 2018, 9, 202.

[18] Hussein, Y. H.; Youssry, M. Polymeric Micelles of Biodegradable Diblock Copolymers: Enhanced Encapsulation of Hydrophobic Drugs. Materials, 2018, 11, 688.

[19] Huang, S.; Jiang, S. Structures and Morphologies of Biocompatible and Biodegradable Block Copolymers. RSC Adv. 2014, 4, 24566−24583.

[20] Castillo, R. V.; Müller, A. J. Crystallization and Morphology of Biodegradable or Biostable Single and Double Crystalline Block Copolymers. Prog. Polym. Sci. 2009, 34, 516−560.

[21] Tharmavaram, M.; Rawtani, D.; Pandey, G. (2017). Fabrication Routes for One-dimensional Nanostructures via Block Copolymers. Nano converg. 2017, 4, 1−13.

[22] Agbolaghi, S.; Abbasi, F.; Abbaspoor, S. Preparation of Polymer Brushes via Growth of Single Crystals of Poly(ethylene glycol)-block-polystyrene Diblock Copolymers Synthesized by ATRP and Studying the Crystal Lateral Size and Brush Tethering Density. Polym. Bull. 2014, 71, 3177−3196.

[23] Abbaspoor, S.; Abbasi, F.; Agbolaghi, S. A Novel Approach to Prepare Polymer Mixed-Brushes via Single Crystal Surface Patterning. RSC Adv. 2014, 4, 17071–17082.

[24] Abbaspoor, S.; Abbasi, F.; Agbolaghi, S. Effects of Various Polymer Brushes on the Crystallization of Poly(ethylene glycol) in poly (ethylene glycol)-b-Polystyrene and Poly(ethylene glycol)-b-Poly(methyl

[Downloaded from isee.iust.ac.ir on 2025-07-27]

[DOI: 10.22068/ijmse.2132]

methacrylate) Single Crystals. J. Polym Res. 2014, 21, 1–8.

[25] Nazari, M.; Agbolaghi, S.; Abbaspoor, S.; Gheybi, H.; Abbasi, F. Arrangement of Conductive Rod Nanobrushes via Conductive–Dielectric–Conductive Sandwiched Single Crystals of Poly(ethylene glycol) and Polyaniline Block Copolymers. Macromolecules 2015, 48, 8947–8957.

[26] Wei, X.; Lv, X.; Zhao, Q.; Qiu, L. Thermosensitive β-Cyclodextrin Modified Poly(ε-caprolactone)-poly(ethylene glycol)-poly(ε-caprolactone) Micelles Prolong the Anti-Inflammatory Effect of Indomethacin Following Local Injection. ActaBiomater.2013, 9, 6953–6963.

[27] Liu, C. B.; Gong, C. Y.; Huang, M. J.; Wang, J. W.; Pan, Y. F.; Zhang, Y. D.; Li, G. Z.; Gou, M. L.; Wang, K.; Tu, M. J.; Wei, Y. Q. Thermoreversible Gel–Sol Behavior of Biodegradable PCL–PEG–PCL Triblock Copolymer in Aqueous Solutions. J. Biomed. Mater. Res. B. Appl. Biomater. 2008, 84, 165–175.

[28] Shi, Y.; Zhu, H.; Ren, Y.; Li, K.; Tian, B.; Han, J.; Feng, D. Preparation of Protein-Loaded PEG-PLA Micelles and the Effects of Ultrasonication on Particle Size. Colloid. Polym. Sci. 2017, 295, 259–266.

[29] Shi, Y.; Huang, W.; Liang, R.; Sun, K.; Zhang, F.; Liu, W.; Li, Y. Improvement of in Vivo Efficacy of Recombinant Human Erythropoietin by Encapsulation in PEG–PLA Micelle. Int. J. Nanomedicine. 2013, 8, 1–11.

[30] Takahashi, Y.; Tadokoro, H. Structural Studies of Polyethers, $(-(CH_2)_m-O-)_n$. X. Crystal Structure of Poly(ethylene oxide). Macromolecules 1973, 6, 672−675.

[31] Hu, H.; Dorset, D. L.Crystal Structure of Poly(iε-caprolactone). Macromolecules 1990, 23, 4604.

[32] Miyata, T.; Masuko, T. Morphology of Poly(l-lactide) Solution-Grown Crystals. Polymer 1997, 38, 4003−4009.

[33] Brandup, J.; Immergut, E. H. Polymer Handbook, Wiley, New York, 1975, 1−1865.

[34] Barton, A. F. M. CRC Handbook of Solubility Parameters and Other Cohesion Parameters, Second Edition, CRC Press, 1991, 1-1600.

[35] Demirel, A.L.; Degirmenci, M.; Yagcı, Y. Atomic Force Microscopy Investigation of Asymmetric Diblock Copolymer Morphologies in Thin Films. Eur. Polym. J. 2004, 40, 1371–1379.

[36] Zheng, J. X.;Xiong, H.; Chen, W. Y.; Lee, K.; Van Horn, R. M.; Quirk, R. P.; Lotz, B.; Thomas, E. L.; Shi, A.-C.; Cheng, S. Z. D. Onsets of Tethered Chain Overcrowding and Highly Stretched Brush Regime via Crystalline−Amorphous Diblock Copolymers. Macromolecules 2006, 39, 641–650.

[37] Abraham, G. A.; Gallardo, A.; Motta, A.; Migliaresi C.; Roman J. S. Microheterogeneous Polymer Systems Prepared by Suspension Polymerization of Methyl Methacrylate in the Presence of Poly(ε-caprolactone). Macromol. Mater. Eng. 2000, 282, 44–50.

[38] Zhang, G.; Zhang, J.; Wang, S.; Shen, D. Miscibility and Phase Structure of Binary Blends of Polylactide and Poly(methyl methacrylate). J. Polym. Sci. B. Polym. Phys. 2003, 41, 23–30.

[39] Laredo, E.;Prutsky, N.; Bello, A.;Grimau, M.; Castillo, R. V.; Müller, A. J.; Dubois, Ph. Miscibility in Poly(L-lactide)-b-Poly(ε-caprolactone) Double Crystalline Diblock Copolymers. Eur. Phys. J. E. 2007, 23, 295–303.

[Downloaded from isee.iust.ac.ir on 2025-07-27]

[DOI: 10.22068/ijmse.2132]